


## Article

# Drying Shrinkage, Sulphuric Acid and Sulphate Resistance of High-Volume Palm Oil Fuel Ash-Included Alkali-Activated Mortars

Ghasan Fahim Huseien <sup>1,\*</sup>, Mohammad Ali Asaad <sup>2</sup>, Aref A. Abadel <sup>3,\*</sup> , Sib Krishna Ghoshal <sup>4,\*</sup>, Hussein K. Hamzah <sup>5</sup>, Omrane Benjeddou <sup>6</sup> and Jahangir Mirza <sup>7</sup>

- <sup>1</sup> Department of the Build Environment, School of Design and Environment, National University of Singapore, Singapore 117566, Singapore
- <sup>2</sup> Department of Civil Engineering, Iraq University College (IUC), Basra 61001, Iraq; mohammad.asaad@iuc.edu.iq
- <sup>3</sup> Department of Civil Engineering, College of Engineering, King Saud University, Riyadh 11421, Saudi Arabia
- <sup>4</sup> Department of Physics, AOMRG, Faculty of Science, Universiti Teknologi Malaysia, Johor Bahru 81310, Malaysia
- <sup>5</sup> Faculty of Industrial and Agricultural Civil Engineering, Technical University of Civil Engineering Bucharest, Bulevardul Lacul Tei 124, Sect. 2, 020396 Bucharest, Romania; hus77top@gmail.com
- <sup>6</sup> Department of Civil Engineering, College of Engineering, Prince Sattam bin Abdulaziz University, Alkharj 16273, Saudi Arabia; benjeddou.omrane@gmail.com
- <sup>7</sup> Department of Civil Engineering, York University, Toronto, ON M4N 3M6, Canada; mirza7861@gmail.com
- \* Correspondence: bdggfh@nus.edu.sg (G.F.H.); aabadel@ksu.edu.sa (A.A.A.); sibkrishna@utm.my (S.K.G.)



**Citation:** Huseien, G.F.; Asaad, M.A.; Abadel, A.A.; Ghoshal, S.K.; Hamzah, H.K.; Benjeddou, O.; Mirza, J. Drying Shrinkage, Sulphuric Acid and Sulphate Resistance of High-Volume Palm Oil Fuel Ash-Included Alkali-Activated Mortars. *Sustainability* **2022**, *14*, 498. <https://doi.org/10.3390/su14010498>

Academic Editor: Constantin Chalioris

Received: 9 December 2021

Accepted: 29 December 2021

Published: 4 January 2022

**Publisher's Note:** MDPI stays neutral with regard to jurisdictional claims in published maps and institutional affiliations.



**Copyright:** © 2022 by the authors. Licensee MDPI, Basel, Switzerland. This article is an open access article distributed under the terms and conditions of the Creative Commons Attribution (CC BY) license (<https://creativecommons.org/licenses/by/4.0/>).

**Abstract:** Nowadays, an alkali-activated binder has become an emergent sustainable construction material as an alternative to traditional cement and geopolymer binders. However, high drying shrinkage and low durability performance in aggressive environments such as sulphuric acid and sulphate are the main problems of alkali-activated paste, mortar and concrete. Based on these factors, alkali-activated mortar (AAM) binders incorporating high-volume palm oil fuel ash (POFA), ground blast furnace slag (GBFS) and fly ash (FA) were designed to enhance their durability performance against aggressive environments. The compressive strength, drying shrinkage, loss in strength and weight, as well as the microstructures of these AAMs were evaluated after exposure to acid and sulphate solutions. Mortars made with a high volume of POFA showed an improved durability performance with reduced drying shrinkage compared to the control sample. Regarding the resistance against aggressive environments, AAMs with POFA content increasing from 0 to 70% showed a reduced loss in strength from 35 to 9% when subjected to an acid attack, respectively. Additionally, the results indicated that high-volume POFA binders with an increasing FA content as a GBFS replacement could improve the performance of the proposed mortars in terms of durability. It is asserted that POFA can significantly contribute to the cement-free industry, thus mitigating environmental problems such as carbon dioxide emission and landfill risks. Furthermore, the use of POFA can increase the lifespan of construction materials through a reduction in the deterioration resulting from shrinkage problems and aggressive environment attacks.

**Keywords:** alkali-activated mortar; palm oil fuel ash; drying shrinkage; sulphuric acid attack; sustainability

## 1. Introduction

The life cycle of a concrete structure depends upon the crucial aspect of durability performance. Acid, chloride and sulphate corrosion are the main factors that affect the durability of concretes, wherein specific working conditions increase the generation of ettringite via gypsum [1,2]. Concrete is demolished when ettringite expands following the aggregation of a specific quantity of ettringite [3,4]. Meanwhile, concrete's strength weakens as the cohesiveness of the calcium-silicate-hydrate product (C-S-H) reduces due to the

presence of biogenic sulphuric acid (BSA) [5]. The recent literature has extensively reported and acknowledged the role of BSA in concrete corrosion [6–8]. A novel comprehension of the corrosion mechanism was developed (Parker’s BSA corrosion mechanism) for concrete, serving as a basis for numerous studies [9,10]. A decrease in the corrosion rate and a barrier against additional acid ingress occurs upon a specific thickness being reached by the reaction-induced gypsum layer [9]. Nonetheless, further corrosion can occur due to the increased surface area that the rough gypsum surface layer generates, as other academics note [11].

Corrosion damage is exacerbated by the production of ettringite that originated from a reaction between gypsum in the concrete and calcium aluminate. Due to continuous corrosion, cracks can form. Upon the tensile strength being surpassed by the internal stress of the ettringite, cracks can occur following expansion [12,13]. When concrete is placed in an alkaline environment, stable ettringite is generated once the gypsum travels to the depths of the non-corroded concrete [14]. Nevertheless, the concept that ettringite acts as an intermediary substance is posited by some researchers, wherein the corrosion layer contains only a marginal quantity of ettringite [15]. In another study, the generation of expansive gypsum is seen as the cause of the reduction in concrete strength once eroded by BSA [16]. The sequence of action by gypsum and ettringite and even their actuality is still the subject of debate within the field, as evidenced by the above.

Recently, more environmentally friendly alkali-activated mortars (AAMs) and concrete have been investigated and developed, leading to the generation of substantially less carbon dioxide (CO<sub>2</sub>) [17,18]. Binders that utilize waste materials such as ground blast furnace slag (GBFS), silica fume (SF), palm oil fuel ash (POFA), FA, metakaolin (MK) and waste ceramic (WCP) are generated via the use of geopolymers when producing concrete in line with the alkaline method, instead of generating high quantities of CO<sub>2</sub> when producing ordinary Portland cement (OPC) [19,20]. Lately, both academic and commercial circles have focused on the development of an OPC alternative. The natural characteristics and capabilities of such alternatives to reduce the emission of CO<sub>2</sub> and resist chemical attacks, fires and heat while demonstrating satisfactory strength and functionality akin to OPC are among the areas that have drawn attention [21–23]. The use of multiple alkaline activators triggers a reaction from various aluminosilicate materials, and this area along with the microstructural classification of such materials have been the focus of certain studies [24,25]. Yet, the proportions of an ecological concrete mix have not been established. Over the past decade, an increasing number of studies have been conducted regarding the generation of ecological mortars and concrete [26–28].

The use of FA as industrial waste stands out above the rest of the various source materials utilized to prepare AAM binders [29,30]. A substantial amount of amorphous silica and alumina resides within FA, which stems from the generation of electricity in thermal power plants when coal burning produces FA as a by-product [31]. Thus, the compatibility of FA as a resource material that generates alkali-activated binders (AABs) is demonstrated by its chemical composition. Multiple studies have investigated the properties and characteristics of FA-based AAMs and their use as possible cementitious materials because they demonstrate stellar durability properties. Their engineering properties make them compatible in multiple construction contexts, as academic works note [32,33]. However, FA-based AAMs present various issues due to their low compressive strength (CS), slow setting time and because temperatures of 40–85 °C are needed for curing. The overall properties of such AAMs are improved via the incorporation of waste materials such as GBFS to address the mentioned issues [34]. Amorphous hydrated alkali alumina-silicate and calcium silicate hydrate are the principal reaction products of alkali-activated cements made from FA and GBFS, respectively [22]. High drying shrinkage (DS), inadequate workability and problems with rapid setting affect alkali-activated GBFS, restricting its usage despite high CS [35]. A decrease in the solution demand alongside improved strength, setting time and workability could take place following the addition GBFS in FA-based AAMs. The durability of mortar in sulphate and a sulphuric acid environment can be decreased due to GBFS unless such a

combination occurs. Moreover, a decrease in the mortar resistance to harsh environments is caused by the high amount of calcium oxide (CaO) in GBFS. Nonetheless, AAM mixtures can end up consuming more energy, emitting more CO<sub>2</sub> and costing more due to the higher GBFS level in the mortar matrix.

The use of agricultural and industrial waste materials in the construction sector has been suggested to overcome the problems associated with the conventional OPC-based concretes [36,37]. Human health hazards have arisen from the dangerous residual industrial and agricultural products that must be effectively disposed of. In recent times, the agricultural residues have been intensively used to make concrete [38,39]. Standard cement materials negatively impact the environment through the significant CO<sub>2</sub> emissions, which highlights the more compatible properties of agricultural waste materials when mixed with concrete [40,41]. In the production stage, the materials typically used consume more energy than POFA, which offers environmental benefits as it is a geopolymer [42]. The efficient use of POFA in additional industries has not been enacted in countries such as Malaysia, where landfills and lagoons are filled with thousands of tons of POFA [43]. Production and transportation costs decrease when utilizing POFA as a partial cement substitute. Additionally, less waste materials in landfills have a positive impact on the environment.

When palm oil is produced by the industries, POFA is also created as a secondary solid waste in the combustion of fibre and oil palm shells, generating biomass energy. Temperatures between 700 and 1000 °C are used to burn the generated solid waste following the extraction of palm oil [44]. It is possible that CO<sub>2</sub> is emitted during the generation of biomass energy following the combustion of fibre and oil palm shells. Nonetheless, utilising the ash that is usually discarded after combustion has taken place is one of the research objectives of this paper. A POFA yield of 5% is generated by the burning process, as per the literature review [40]. Abandoned sand quarries, swamp lands and the area close to the palm oil mill are where the generated ash from the burning procedure is most frequently thrown away [45,46]. Larger particles and unburnt fibres are separated and discarded via a sieve to attain the POFA in the palm oil mill. Due to the high levels of aluminates and silicates within POFA, it is classified as a pozzolanic material [47]. Iron oxide (Fe<sub>2</sub>O<sub>3</sub>) and aluminium oxide (Al<sub>2</sub>O<sub>3</sub>) are among the pozzolanic components within POFA; while, by volume, between 50 and 60% of the chemical composition of POFA consists of SiO<sub>2</sub> [48,49]. The value for loss of ignition (LOI) and the content of carbon decreases after heating takes place, as per another study [40].

The burning of palm oil husks and palm kernel shells, among other waste materials, causes the production of the ash family materials, POFA being one of them [50]. Ever increasing annual POFA and ash deposits in landfills have gradually become an encumbrance [51]. Thus, the hazards of such waste materials can be circumvented by formulating a manner in which to use these materials. The possible incorporation of palm oil fuel ash into concrete and an examination of the former's properties were carried out in a study in the 1990s [52], wherein POFA between 10 and 50% was substituted for OPC. Upon 20 to 50% of the cement being substituted by POFA, the CS of the samples was diminished. The resistance of the concrete against sulphate attacks was improved via the addition of POFA [53]. How the pozzolanic reaction with cement paste is impacted by POFA was investigated in another study [54]. The cement paste mixes had a water to binder ratio (W/B) of 0.35 and cementitious material weights of 10, 20, 30 and 40% of Ground River Sand (GRS) or Ground Palm Oil Fuel (GPOFA) substituting for the OPC. With POFA having a higher fineness, the concrete mixtures and cement paste were impacted more significantly by the POFA.

It is known that concrete durability is negatively impacted by the formation of micro-cracks in the specimen's surface, which is provoked by the drying out of the hardened concrete specimen, otherwise known as drying shrinkage. Following the preparation of the concrete, the first three or so days are when water evaporation typically occurs the most on the concrete surface, which leads to drying shrinkage [50,55,56]. Samples that substituted in 20 to 50% POFA were found to have higher shrinkage than the control

sample and samples with 10% POFA substituted in, where the latter two had equivalent shrinkage results [57]. Once concrete casting has taken place, the initial 90 days are when the most drying shrinkage typically occurs, amounting to 70% of the total drying shrinkage. The drying shrinkage and micro-strain of the control specimen gave a value of  $557 \times 10^{-6}$ , which was greater than the samples that substituted in 10, 20 and 30% POFA that demonstrated a micro-strain of  $525 \times 10^{-6}$ ,  $505 \times 10^{-6}$ , and  $494 \times 10^{-6}$ , respectively. Conversely, the control cement concrete sample was found to have a lower shrinkage strain than concrete samples with POFA added to them in another academic work [58]. BS 812: Part 120 served as the basis for analysing prism samples measuring 25 mm  $\times$  25 mm  $\times$  285 mm in size to deduce their concrete shrinkage by utilising a length comparator, as per a recent study [59]. The cement mortar mix was found to produce lower drying shrinkage values than the mortar specimens mixed with POFA. The control specimen produced a higher micro-strain value of  $785 \times 10^{-6}$  in comparison with the concrete samples with 10, 20 and 30% ultrafine palm oil fuel ash (UPOFA) substituted in, which demonstrated values of  $707 \times 10^{-6}$ ,  $670 \times 10^{-6}$  and  $645 \times 10^{-6}$ , respectively, as per another academic work [60]. Findings that were equivalent were reported in a separate study [61]. The DS was reduced by 7.5% due to the incorporation of 30% nanosilica and POFA [62].

Traditional Portland cement can be effectively substituted by alkali-activated binders. Not only can alkali-activated binders save energy and reduce CO<sub>2</sub> emissions, but they can also augment the durability performance of concrete as well as aid in resolving the landfill problems. It is well-known that extensive quantities of natural, industrial and agriculture wastes are created every year, of which a significant amount is used in landfills. It is, thus, more appropriate to reuse this waste efficiently. In recent years, dedicated efforts have been made to increasingly use the alkali-activated binders (AABs) as a sustainable alternative to the conventional OPC in order to enhance the durability performance and reduce the environmental problems. However, the issues related to high drying shrinkage and low durability performance against a sulphuric acid environment are the main hindrance for large-scale manufacturing and penetration into the marketplace. With this perception, we analysed the impact of a high volume of POFA (as a replacement of GBFS and FA) on the durability performance of the proposed AAMs. These AAMs activated with a low concentration of alkaline solution were prepared by replacing GBFS with a high volume of POFA and FA. The CS, microstructures, drying shrinkage and resistance to the acid and sulphuric attack of the AAMs were examined to evaluate their durability performance.

As abovementioned, this research intends to generate new information on the use of multi-blend AAM by means of systematic methods of preparing samples from waste materials economically, appropriately and carefully characterizing materials, and subsequent data analyses valuable for the progress of standard specifications of ternary-blend AAMs toward diversified realistic applications. This generated knowledge is expected to provide the advancement of environmental amiable and inexpensive AAMs for a broad array of uses in the construction sectors. This would be greatly advantageous for sustainable development worldwide, where wastes disposal problems toward land filling can be avoided and minimized. The new findings of this research are believed to render a basis for further studies and better knowledge on the behaviour of ternary-blend AAMs obtainable from the waste material in a cheap and environmental affable manner.

## 2. Methodology

### 2.1. Materials

Palm oil mills produce the waste material POFA, as previously mentioned. Kilang Sawit PPNJ Kahang, which is based in Johor in Malaysia, served as the ash collection point for POFA. For an entire day, an oven at a temperature of 105 °C was used to dry the POFA once the larger particles were discarded via a 600-micrometre sieve. The efficacy of the POFA was further enhanced via the removal of larger particles by using a 300-micrometre sieve. Subsequently, fine particles were produced through the use of the

Los Angeles Abrasion milling machine after the remaining POFA particles were ground for 6 h (Figure 1), wherein a drum containing 15 stainless balls (each with a diameter of 50 mm) with controlled speed (which ranged from 32 to 35 rpm) was used. Every hour, the particle fineness that was impacted by the 6 h of grinding was assessed. The period of grinding diminished the number of remaining particles put through a 45-micrometre sieve. Following the completion of the grinding period, the 45-micrometre sieve was used for all the POFA specimens. The finer the particles of binder materials are, the stronger the microstructure density and engineering properties of the concrete and mortar are. In line with ASTM C618-15 stipulations, the core properties of POFA under the Class F pozzolana group are illustrated in Table 1. The assessment of the specific gravity, particle size, colour and specific surface area (physical properties) were, correspondingly, 1.96, 8.2  $\mu\text{m}$ , dark grey and 23.1  $\text{m}^2/\text{g}$ . The physical and chemical characteristics of the raw materials together with the compositions are known to greatly influence the AAMs' performance. X-ray fluorescence (XRF) spectroscopy was used to detect the chemical compositions of POFA, as summarized in Table 1. The main oxides' compositions were silica, calcium, potassium, magnesium and aluminium in the presence of 64.2, 10.2, 8.6, 5.9 and 4.3 weight %, respectively.



**Figure 1.** POFA lab treatment.

Ipoh in Malaysia served as the collection point for GBFS that enabled the production of the binder without cement. No laboratory treatment was needed to use the mentioned resource material. The pozzolanic and cementitious properties of GBFS make it stand out in comparison to other supplementary binding materials. Upon mixing and exposure to water, the hydraulic reaction generates an off-white colour in the GBFS. In line with ASTM C618 stipulations, GBFS satisfies the criteria for a pozzolanic material and roughly 90% of its content is made up of alumina and calcium silicate. The chemical composition of GBFS is demonstrated in a condensed form in Table 1. These properties are beneficial for the alkali-activated mortar production, wherein the specific surface area, specific gravity and average particle size were, correspondingly, 13.6  $\text{m}^2/\text{g}$ , 2.89  $\text{g}/\text{cm}^3$  and 12.8  $\mu\text{m}$ . Depending on the XRF results, the calcium, silica and aluminium oxides were found to be primary elements, which are 93.5% of the total chemical composite of GBFS. As a resource of aluminosilicate, FA, with little Ca content, was collected from a power station (Tanjung bin, Malaysia) to design the proposed AAMs. The obtained material met the ASTM C618 requirement for N class pozzolan and F class FA, which was grey in colour with a density of 2200  $\text{kg}/\text{m}^3$ , specific surface area of 18.1  $\text{m}^2/\text{g}$  and average diameter of 10  $\mu\text{m}$ . For the

chemical composition, silica (57.2%) and aluminium oxides (28.8%) were observed to be the main elements.

**Table 1.** Chemical and physical traits of POFA, GBFS and FA.

Material	POFA	GBFS	FA
Physical characteristics			
Density (kg/m <sup>3</sup> )	1900	2900	2200
Specific gravity	1.9	2.9	2.2
Surface area-BET (m <sup>2</sup> /g)	23.1	13.6	18.1
Average diameter (µm)	8.2	12.8	10
Chemical composition, weight %			
Silica oxide (SiO <sub>2</sub> )	64.20	30.8	57.20
Aluminium oxide (Al <sub>2</sub> O <sub>3</sub> )	4.25	10.9	28.81
Iron oxide (Fe <sub>2</sub> O <sub>3</sub> )	3.13	0.64	3.67
Calcium oxide (CaO)	10.20	51.8	5.16
Magnesium oxide (MgO)	5.90	4.57	1.48
Potassium oxide (K <sub>2</sub> O)	8.64	0.36	0.94
Sodium oxide (Na <sub>2</sub> O)	0.10	0.45	0.08
Sulphur trioxide (SO <sub>3</sub> )	0.09	0.06	0.10
Loss of ignition (LOI)	1.73	0.22	0.12

Figure 2 displays the X-ray Diffraction (XRD) profiles of various constituents of AAMs. The intense diffraction peaks in the range of 16° and 30° were due to the presence of crystalline alumina and silica in POFA and FA. However, the presence of mullite phases and crystalline quartz was seen as the cause for separate crystalline peaks. The actual amorphous nature of GBFS was confirmed by the presence of a wide hump and the altogether lack of sharp crystalline peaks. The reactive calcium and silica within GBFS make up one of the key elements in the creation of GBFS. The preparation and production of alkali-activated mortar seems to be complemented by the high levels of reactive amorphous calcium and silica within GBFS. Nonetheless, the low level of SiO<sub>2</sub> in GBFS is an issue that can only be addressed via the addition of POFA and FA.

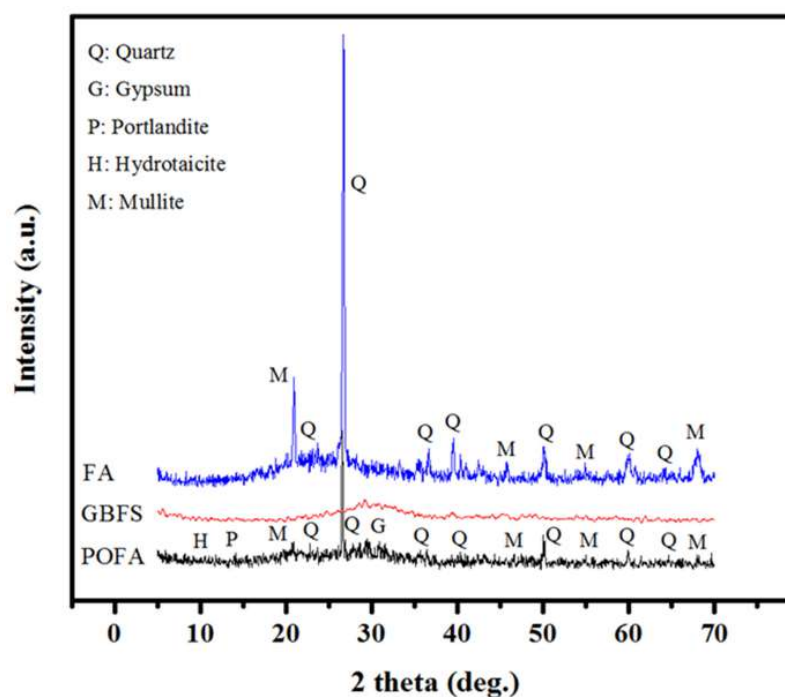


**Figure 2.** XRD profiles of POFA, GBFS and FA.

In this study, all the samples were produced using natural river sand containing silica, which served as the fine aggregate in each mortar mixture. In line with ASTM C117, any silt or other contaminant matter in the sand was removed by washing. Following the washing process, the sand was oven-dried for a period of twenty-four hours at a temperature of 60 °C before establishing the values for specific gravity (2.6) and fineness modulus (2.9) of the sand. To prepare the alkaline activator solution, analytical grade sodium hydroxide (NH) 98% purity pellets and sodium silicate solution (NS) made up of SiO<sub>2</sub> (29.5 weight %), Na<sub>2</sub>O (14.70 wt%) and H<sub>2</sub>O (55.80 wt%) were used in this study. As shown in Figure 3, the pellets were placed in water to dissolve in order to create the NH solution with a concentration of 4 M. This was cooled for a period of 24 h before mixing it with NS solution to create the alkaline solution (S) with a solution modulus (SiO<sub>2</sub>:Na<sub>2</sub>O) of 1.02. All alkaline solutions maintained a low NS:NH ratio of 0.75 in order to minimize the adverse environmental effect of sodium silicate (Na<sub>2</sub>SiO<sub>3</sub>).



**Figure 3.** Alkaline activator solution preparation stages.

### 2.2. Mixes Design and Specimens' Preparation

A high volume of POFA incorporating GBFS and FA with various ratios was used to prepare the AAMs' specimens. A mixture containing GBFS and FA as binders with a ratio of 50:50 was adopted as the control sample. Then, the GBFS was replaced by a high volume of POFA and FA, as shown in Table 2. The ratios of alkali solution to binder (S:B), binder to fine aggregate (B:A) and sodium silicate to sodium hydroxide for the designed AAMs were fixed to 0.40, 1.0 and 0.75, respectively. First, 50% of the binders (POFA, GBFS and FA) were mixed for 2 min in dry conditions. Then, the resultant mix was added the sand and mixed for an extra 2 min. Before adding the alkaline solution, the other 50% of the binder was added and mixed until a homogenous state was achieved. Finally, the cold alkali solution was added and the whole matrix of the binder, fine aggregates and solution were mixed in machine for another four minutes. Immediately, the fresh mortar was casted in two layers by being kept in the vibration table for 15 s during each layering to escape air voids. The prepared specimens were de-moulded after 24 h and left in the same environment (at  $27 \pm 1.5$  °C and 75% relative humidity) until the testing time.

### 2.3. Procedure of Tests

Following ASTM C579, standard cube specimens of dimension (50 mm × 50 mm × 50 mm) were prepared, and the CS test was carried out at curing ages of 1, 3, 7, 28, 56, 90, 180 and 360 days, as per ASTM C109 [63]. To measure the drying shrinkage (DS) of the suggested mixtures, prism specimens with 40 mm × 40 mm × 250 mm dimensions were prepared. After various curing ages for each mixture, three samples were tested, and the average value was adopted. A consistent loading rate of 2.5 kN/s was applied to the AAMs' specimens. The effects of sulphuric acid (H<sub>2</sub>SO<sub>4</sub>) and sulphate (MgSO<sub>4</sub>) on the AAMs were evaluated, wherein 10% H<sub>2</sub>SO<sub>4</sub> and MgSO<sub>4</sub> solutions were prepared in deionized water (DIW). Six specimens of each mix were weighed at 28 days and their ultrasonic pulse

velocity (UPV) was recorded before immersing into the sulphuric and sulphate solutions for another 360 days. The impact of the high level of POFA on AAMs resistance against the  $H_2SO_4$  and  $MgSO_4$  solutions were evaluated in terms of the loss of strength, weight and UPV as well as the edges and surface deterioration. The solution was altered every 2 months to keep the pH level constant during the experiment (Figure 4) [2]. Based on the ASTM C267 specifications [64], the durability performance of the prepared specimens was evaluated after 180 and 360 days from the immersion date. The major reason for the  $H_2SO_4$  and  $MgSO_4$  solution attack was due to the penetration of sulphate ion  $(SO_4)^{2-}$  and cations of magnesium, calcium or sodium into AAMs.

**Table 2.** Proposed alkali-activated mixes design.

Mix Code	Binder, weight %			S:B	B:A	NH <sub>3</sub> Molarity	NS:NH	Solution Modulus (Ms)
	POFA	GBFS	FA					
AAM <sub>1</sub>	0	50	50	0.40	1.0	4.0	0.75	1.02
AAM <sub>2</sub>	50	50	0	0.40	1.0	4.0	0.75	1.02
AAM <sub>3</sub>	50	40	10	0.40	1.0	4.0	0.75	1.02
AAM <sub>4</sub>	50	30	20	0.40	1.0	4.0	0.75	1.02
AAM <sub>5</sub>	50	20	30	0.40	1.0	4.0	0.75	1.02
AAM <sub>6</sub>	60	40	0	0.40	1.0	4.0	0.75	1.02
AAM <sub>7</sub>	60	30	10	0.40	1.0	4.0	0.75	1.02
AAM <sub>8</sub>	60	20	20	0.40	1.0	4.0	0.75	1.02
AAM <sub>9</sub>	70	30	0	0.40	1.0	4.0	0.75	1.02
AAM <sub>10</sub>	70	20	10	0.40	1.0	4.0	0.75	1.02

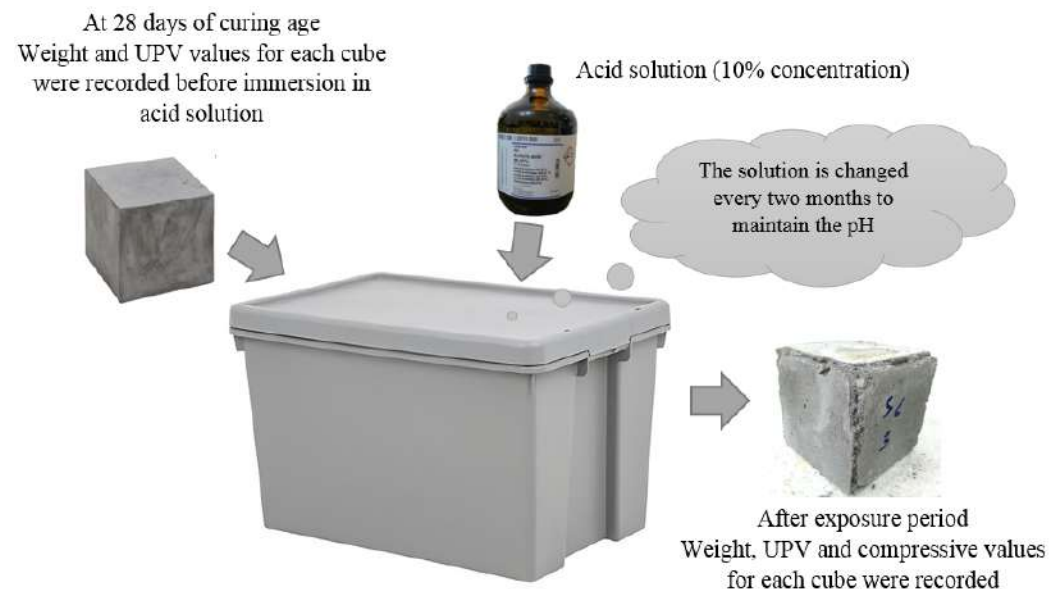


**Figure 4.** Sulphuric and sulphate tests' procedure.

After the CS test, the central portion of every specimen was taken and pulverized. The microstructures of each sample were examined using an XRD measurement, scanning electron microscope (SEM) and Fourier transform infrared (FTIR) spectrometer. The presence of amorphous and other phases in the sample were determined using the MDI Jade software version 6.5 and Match3. XRD patterns were scanned in the angular range of  $5\text{--}60^\circ$  at a step size of 0.02 and a speed of 0.5 s/step, wherein brass stub type sample holders were used to place the powdered AAMs. For the SEM measurement, samples were dried for 5 min under IR radiation and then a Blazer sputter coater (BAL-TEC SCD 005 Sputter Coater machine) was used to cover each specimen with gold. The SEM micrographs were recorded at 20 kV with  $1000\times$  magnification (Hitachi S-3400N). The room temperature FTIR spectra (in the range of  $400\text{--}4000\text{ cm}^{-1}$ ) of each AAM were measured to examine the



presence of various chemical functional groups. The scanning electronic image (SEM)/FTIR analysis was performed on AAMs cured at 28 days of age.

### 3. Results and Discussion

#### 3.1. Strength Performance

The distinct POFA to GBFS and FA ratios regarding the alkali-activated mortar's CS are illustrated in Figure 5. The CS of the specimens cured between 1 and 360 days were impacted substantially by the varying levels of POFA and FA substituting the GBFS in the range of 0 to 70%. At 1 day of age, the CS decreased by 19.9 MPa, going from 38.7 to 18.8 upon the POFA increasing from 0 to 50%. Within the alkali-activated matrix, the decrease in alumina and calcium content and increase in silicate content could explicate the decrease in CS when the POFA level rises.

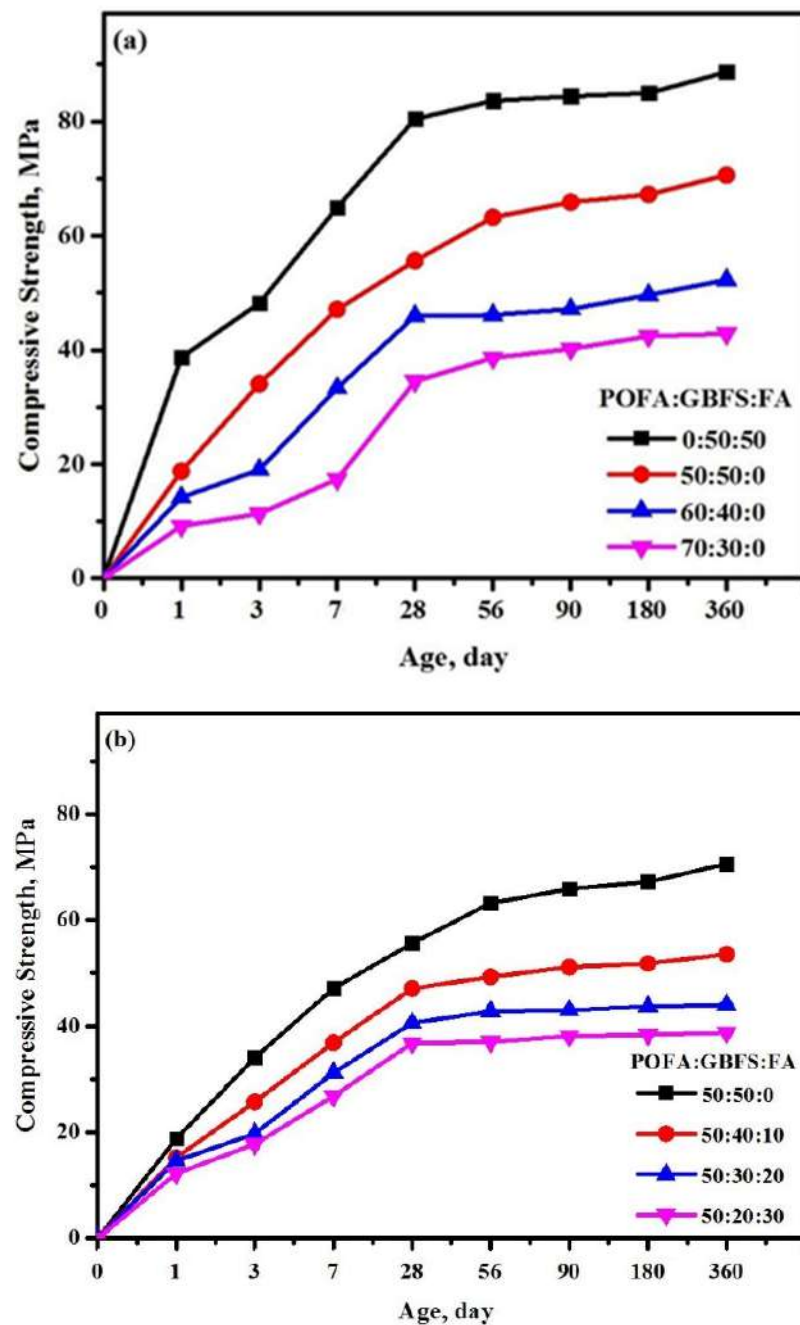


Figure 5. Cont.

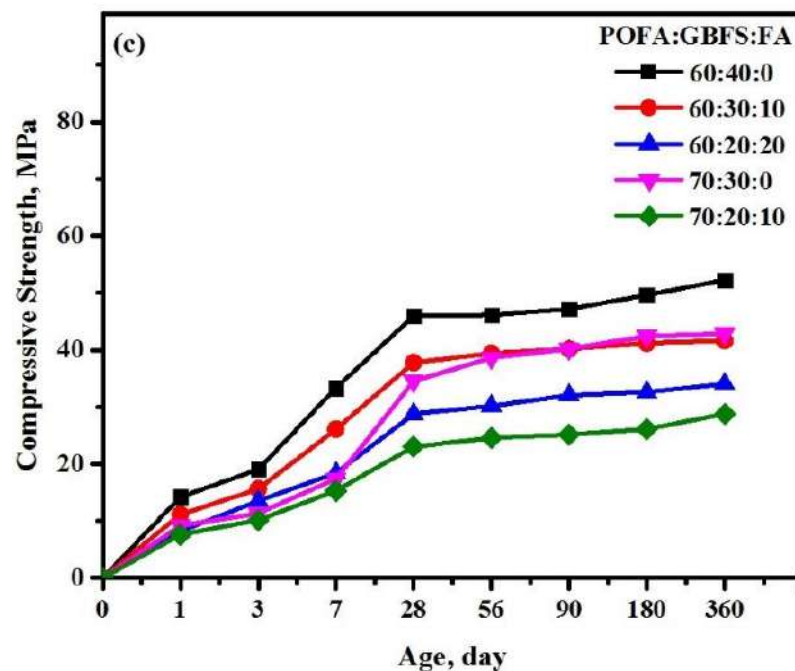


Figure 5. Impact of POFA level on the CS of AAMs designed with GBFS and FA (a) 0% POFA (b) 50% POFA (c) 60 and 70% POFA.

Figure 6 illustrates how a high  $\text{SiO}_2$  to  $\text{Al}_2\text{O}_3$  ratio reaching a maximum of 8.6 occurred when the quantity of POFA augmented. Due to the reactivity of  $\text{Al}_2\text{O}_3$  being lower than  $\text{SiO}_2$ , the generation of C-(A)-S-H gel was impacted as a result [65,66]. The level of CS and calcium oxide decreased, where the latter dropped from 28.5 to 22.7%, along with the production of C-A-S-H and C-S-H gels as the heightened level of POFA rising from 0 to 70% negatively impacted such features. When the POFA content rose from 50 to 70%, the CS of alkali-activated mortars decreased by 21.1 MPa, dropping from 55.6 to 34.5 in 28 days. Other curing ages demonstrated the same pattern of higher levels of POFA causing reductions in CS. Nonetheless, a reduced CS was observed when the GBFS to POFA ratio was higher. It can be deduced that low levels of CaO leads to a diminishing formation of the calcium aluminium silicate hydrate (C-A-S-H) and C-S-H gel that stems from higher levels of POFA. When 70% POFA was substituted in at 360 days, the CS of AAMs produced its lowest value of 42.9 MPa.

The effect of replacing the FA with GBFS for three different high volume POFA contents of 50, 60 and 70% on the AAMs' CS is illustrated in Figure 5b,c, respectively. The CS varied inversely with the FA contents. For a higher ratio of FA to GBFS, the CS was lower. An increasing content of FA that caused a reduction in the C-S-H and C-A-S-H product was due to the influence of low content of calcium oxide (Figure 6). A lower strength was observed for the FA of the GBFS that was replaced with 70% POFA (Figure 5c), which presented 23.1 MPa compared to 28.8 and 36.8 MPa at 28 days with a 60 and 50% POFA level, respectively.

Figure 7 illustrates the XRD patterns of the AAMs designed with various levels of POFA. The existence of glassy phases and the poor crystallinity of GBFS with POFA favoured their strong reaction, generating more reaction products. A nascent quartz peak at  $18^\circ$  demonstrated a higher peak intensity of the quartz that was present between  $16.4^\circ$  and  $28^\circ$  following the POFA content increase from 0 to 70%. Notably, when the POFA content increased to 70% from 50%, a quartz peak substituted the C-S-H peak at  $27.8^\circ$ . A mullite peak replaced the calcite peak at  $51^\circ$  and a hydrocalcite and mullite peak replaced the nepheline peak at  $34^\circ$  and  $24^\circ$ , respectively, following the rise in POFA content, demonstrating significant changes in the XRD pattern. As illustrated in Table 1, high potassium ( $\text{K}_2\text{O}$ ) levels of 8.6% catalysed a muscovite ( $(\text{Al}_2\text{O}_3)_3(\text{SiO}_2)_6(\text{H}_2\text{O})$ ) peak at

36.5° with other novel crystalline XRD quartz-related peaks appearing at 18°, 40° and 51° when 70% of the POFA content was present in the alkali-activated mortars. It was observed that the rise in the POFA level to 70 from 0% caused the CS of the alkali-activated mortars to drop from 80.5 to 34.5 MPa, while the formation of C–S–H similarly dropped, and the intensity of the quartz peaks were improved.

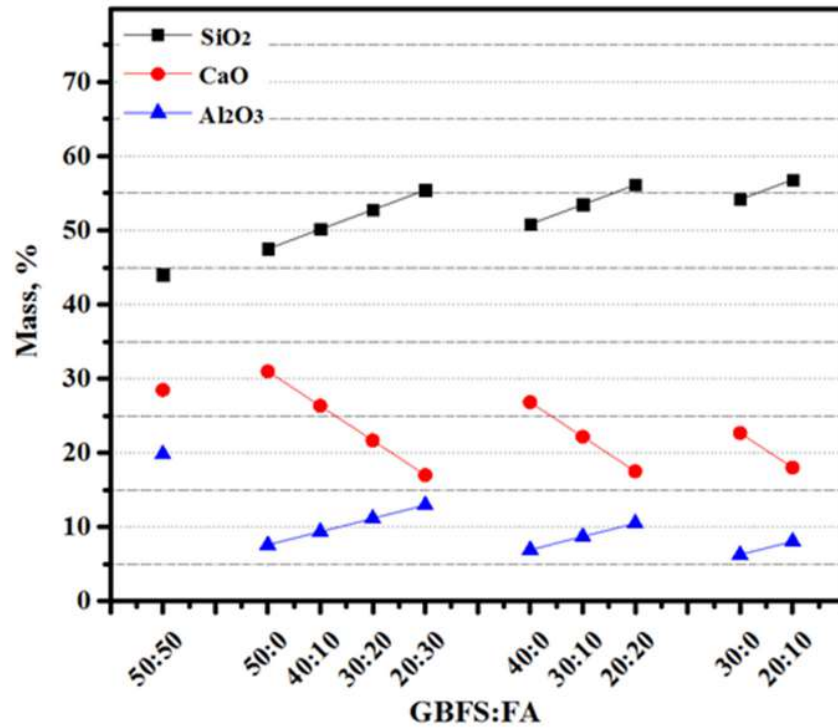


Figure 6. GBFS and FA ratio dependent variation of silica, calcium and aluminium oxides content.

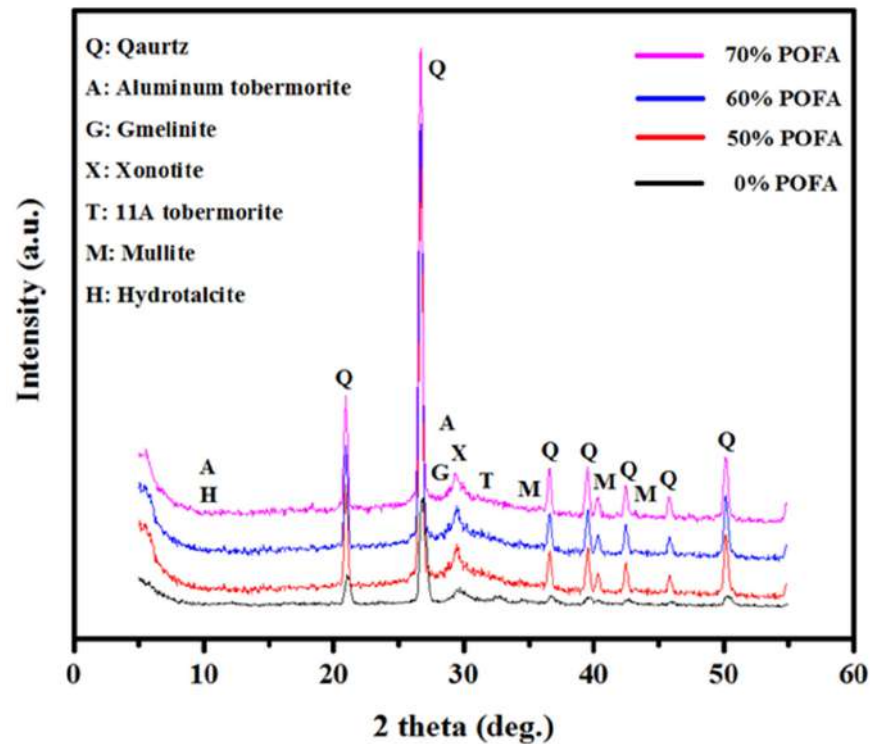
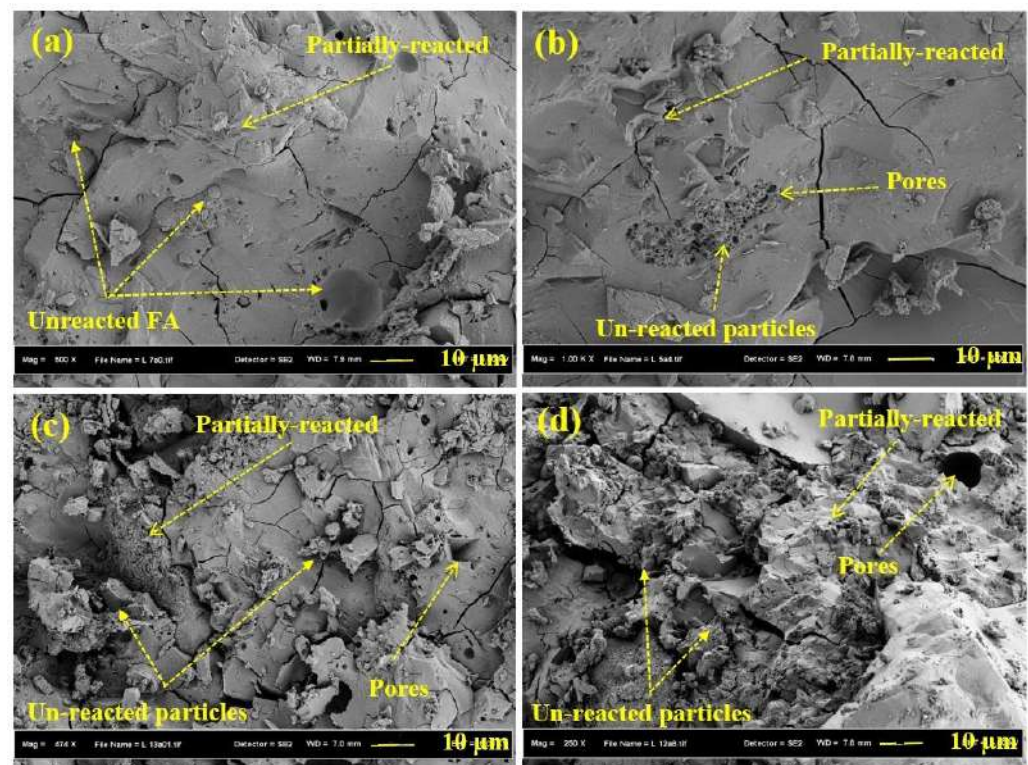


Figure 7. Effect of POFA content on AAMs' XRD patterns.

Figure 8 illustrates the SEM images of AAMs at 28 days prepared with various levels of POFA (0, 50, 60 and 70%). The formation of a strong bond between the unreacted or partially reacted POFA was noticed. The specimen without POFA did not show any cracks at the interfaces (Figure 8a). However, as the POFA level increased from 50 to 70%, the polymer network bonds became weaker, leading to the structural deterioration through the generation of more pores. With an increasing POFA level, the concentrations of the non-reactive particulates were enhanced (Figure 8d) and the generation of C–A–S–H and C–S–H gel products was influenced by the presence of a high quantity of silicate and low amount of calcium, leading to the production of less dense muscovite, mullite and hydrotaicite gels than C–(A)S–H gel. Moreover, much amount of silica remained non-reacted. The poor structure of the AAMs with a high content of POFA (70%) revealed the lowest strength (34.5 MPa) compared to the other samples.



**Figure 8.** SEM of AAMs specimens containing various level of POFA: (a) 0%, (b) 50%, (c) 60%, (d) 70%.

Figure 9 shows the FTIR spectra of the studied AAM after 28 days of curing. The band assignments of the recommended AAMs and their associated FTIR spectral peak locations are demonstrated in Table 3. Following the addition of POFA at 50, 60 and 70% in AAMs, the stretching vibrations of Si–O–Al emerged at 956.9, 963.1 and 964.8  $\text{cm}^{-1}$ , respectively. The mixtures under investigation demonstrated significant structural alterations following higher levels of POFA being added. The higher content level of  $\text{SiO}_2$ , as well as a decrease in C–(N)–A–S–H and C–S–H gel production, could explicate this. The mechanical strength of the alkali-activated mortar samples decreased and the geopolymerization process was delayed, while the structure’s strength increased as a result of the structural changes in the gel formation [67]. The asymmetric stretch of the H–O–H linkage produced wide bands around 3353 and 3360  $\text{cm}^{-1}$ . At the same time, the hydrated reaction products could lead to the bending vibration of the –OH group, which, in turn, explicate the appearance of bands around 1640 and 1648  $\text{cm}^{-1}$ . A geopolymerization reaction involving water in the AAMs and the alkali-solution-induced products is signified by the lack of the mentioned bands within specimens containing un-reacted GBFS and POFA constituents [68].

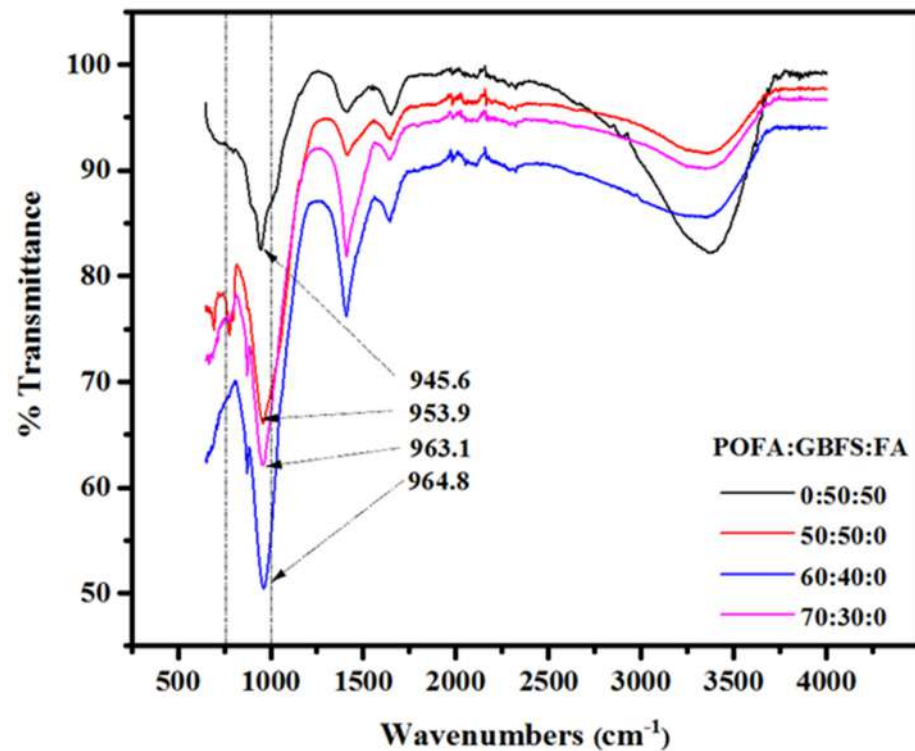


Figure 9. FTIR of AAMs prepared with various of POFA content.

Table 3. FTIR spectral analyses of the proposed AAMs.

Mix			$f_c$ (MPa)	Band Assignments and Positions ( $\text{cm}^{-1}$ )				
POFA:GBFS:FA	Si/Al	Ca/Si		Al–O	Si–O	$\text{AlO}_4$	CSH	C(N)ASH
0:50:50	2.22	0.65	80.6	671.7	690.9	755.3	871.4	945.6
50:50:0	6.25	0.65	55.64	652.5	691.5	805.7	872.1	956.9
60:40:0	7.32	0.53	45.96	653.1	692.5	810.3	872.7	963.1
70:30:0	8.63	0.42	34.53	655.4	693.1	822.5	873.1	964.8

### 3.2. Drying Shrinkage

Figure 10 displays the mean DS values of AAMs enclosing a high volume of POFA. The rate of shrinkage was high during the early stages, up to 28 days, and the rate decreased after this age. With the inclusion of the high volume POFA in alkali-activated matrix at 50 to 70%, the DS values at an early stage (3 days) tend to decrease from 246.1 to 197.6 macrostrain, respectively. A similar trend of results was observed for the specimens evaluated at 28 days of curing age and the values of DS dropped from 410.3 to 359.8 macrostrain with the increase in the POFA content from 50 to 70%. Ultimately, at 180 days, the DS values of AAMs containing GBFS of 50 to 70% was reduced from 497.2 to 431.7 macrostrain, respectively.

For each level of high volume POFA content, it was found that replacing GBFS with FA led to a decrease in the drying shrinkage values for all ages. At an early age (3 days), it was observed for the specimens prepared with 50% POFA that replacing the GBFS with 10 to 30% FA positively affected the reduction in the values of drying shrinkage from 461.1 macrostrain to 219.2 to 175.1 macrostrain, respectively. A similar trend of results was found for the specimens evaluated at 28 and 180 days and the values of shrinkage decreased with an increasing amount of FA as a GBFS replacement. The results of DS of the specimens containing 60 and 70% POFA showed that the reduction in GBFS content by replacing it with FA led to a decrease in the drying shrinkage value. The lowest DS values were recorded at 3, 28 and 180 days for AAMs prepared with 50% POFA, 20% GBFS and 30% FA that showed 175.2, 319.6 and 401.2 macrostrain, respectively. The obtained reduction in DS

values with increasing POFA and FA levels can be ascribed to the production of exceedingly inter-linked capillary-types of networks inside the mortar matrix. The substitution of GBFS by various levels of POFA and FA caused the reduction in CaO level in the mortar due to the lower CaO contents in POFA and FA compared to GBFS. Consequently, this reduction in the CaO content in the AAMs could decrease the hydration reaction rate; thereby, the mortars prepared with high levels of POFA and FA showed lower DS values compared to the one designed with GBFS of 50% [69].

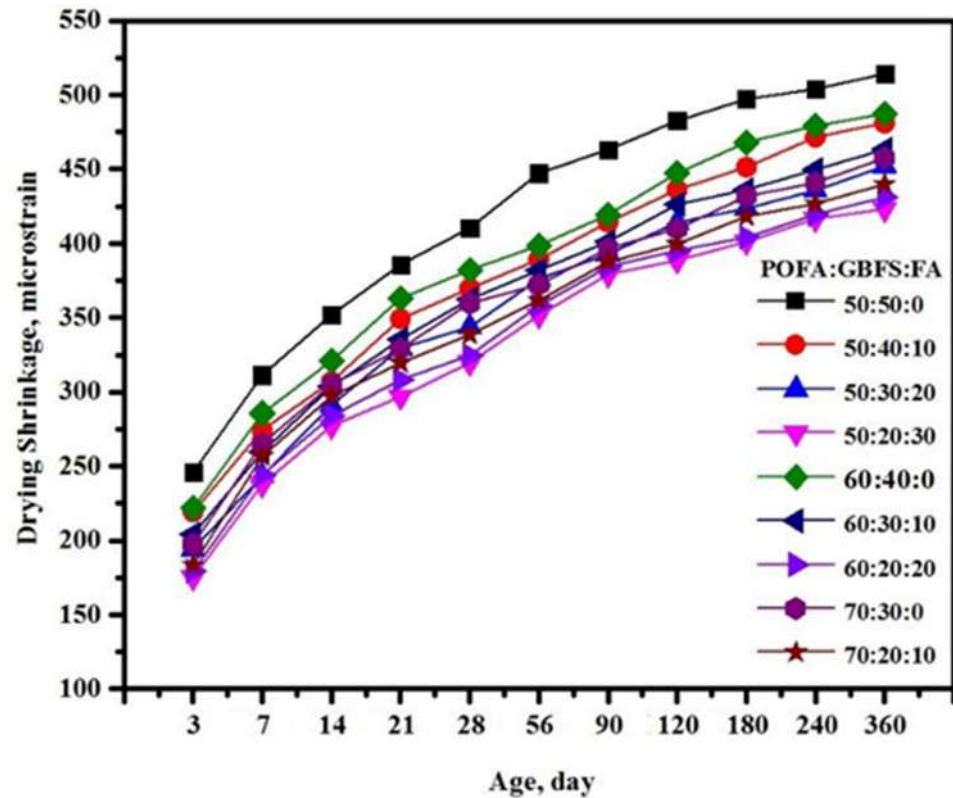


Figure 10. Effect of POFA:GBFS:FA ratios on drying shrinkage of proposed mortars.

### 3.3. Sulphuric Acid Resistance

Figure 11 illustrates that the residual CS of the AAMs and their sulphuric acid resistance are impacted in a synergistic manner by POFA, GBFS and FA. The resistance of the recommended AAMs and their matrixes to sulphuric acid is significantly enhanced by substituting the GBFS for higher levels of POFA and FA. After 180 days from the immersion date, the residual CS rose to 83% from 52.4% after the POFA level also rose to 70% from 50%. Hence, sulphuric acid resistance is enhanced via the substitution of GBFS for higher levels of POFA in the AAMs. A similar trend of results was evaluated after 360 days from the exposed date, and the loss of strength tended to decrease as the amount of POFA as a GBFS replacement increased. The residual CS of the AAMs was enhanced from 36.6 to 75.6% when the POFA levels increased from 50 to 70%, respectively. The results of replacing GBFS with FA in the AAMs showed a positive effect on the resistance of the sulphuric attack and enhanced the proposed mortars' durability performance. The residual CS values of the AAM prepared with 50% POFA were improved from 36.6 to 49% with the corresponding increase in the FA replacement for GBFS from 0 to 30%. The AAMs prepared with a high volume of POFA (70%), 20% GBFS and 10% FA showed the lowest loss values of CS of 8.7 and 17.7% after a 180- and 360-day immersion in the acid solution, respectively. In addition to the residual CS, weight loss is also broadly accepted as an indicator for assessing the resistance of geopolymer specimens to an acid attack [70].

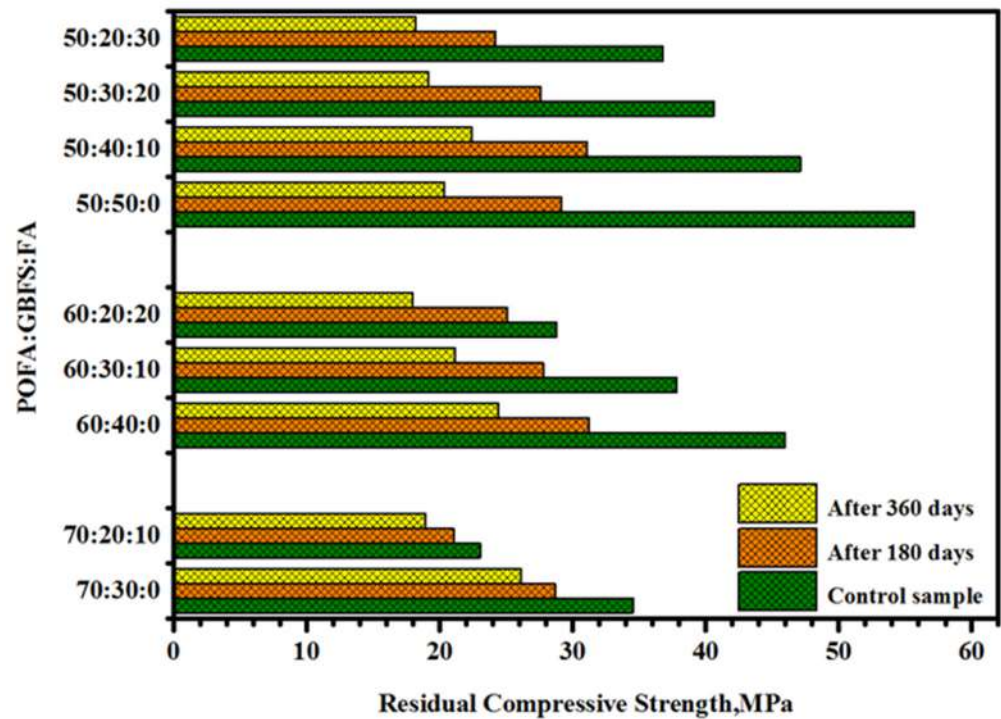


Figure 11. Residual CS of AAMs with high POFA content after immersion in 10% H<sub>2</sub>SO<sub>4</sub> solution.

Figure 12 shows the results of weight loss of AAM specimens exposed to an acid attack. An increase in the POFA content in AAMs from 50 to 70% led to a reduction in the weight loss from 0.2 to 0.12%, respectively. A similar trend of reduced weight loss was observed with FA replacing GBFS; the increase in the FA replacing the GBFS content in 50% POFA alkali-activated specimens from 0 to 3% has reduced the weight loss from 0.20 to 0.13%, respectively. The increased POFA and FA content in alkali-activated matrixes has reduced the calcium oxide content and restricted the gypsum product [71].

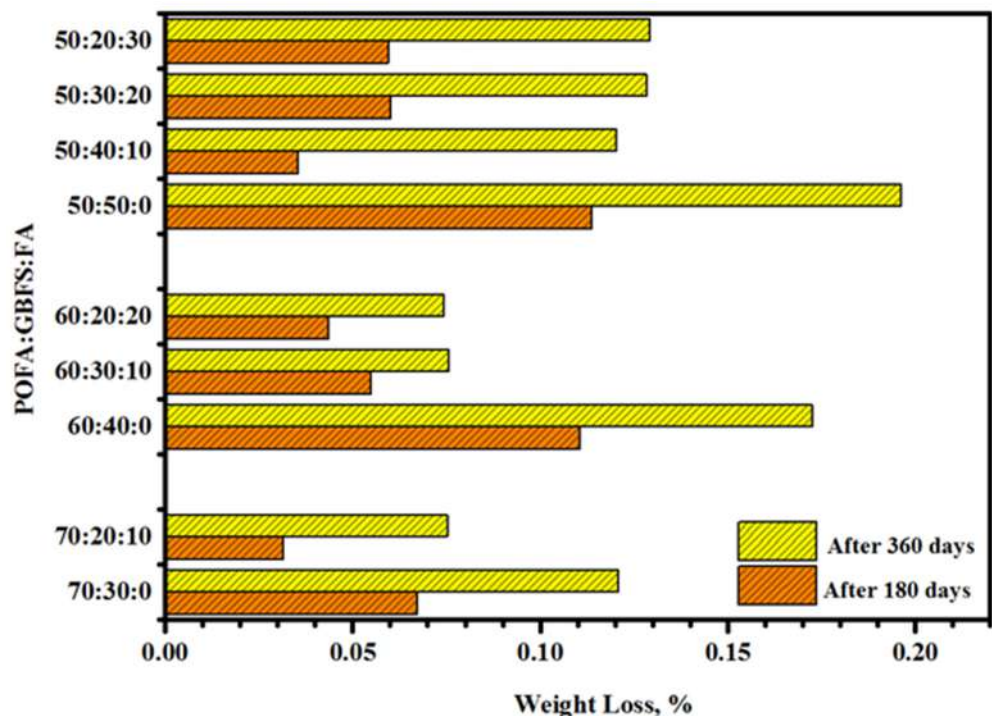


Figure 12. Weight loss of AAMs with high POFA content after immersion in 10% H<sub>2</sub>SO<sub>4</sub> solution.

Figure 13 depicts the effect of a high volume of POFA on the ultrasonic pulse velocity of AAMs after immersing in sulphuric acid solution. An increase in the POFA level from 50 to 70% as the GBFS replacement led to the enhancement of the durability performance and reduction in the internal deterioration. After 180 days exposed to an acid solution, the loss in UPV readings was reduced from 11.8 to 1.6% with an increasing POFA content in the alkali-activated matrix. Comparable results were obtained when the AAMs were exposed to an acid solution for 360 days and the loss on UPV readings dropped from 18.8 to 2.7% when the POFA content rose from 50 to 70%, respectively. At each level of high volume POFA content, replacing GBFS with FA positively enhanced the specimens' durability performance at 180 and 360 days. At the 50% POFA level, the specimens evaluated after 360 days of exposure to an acid solution showed a reduction in the UPV readings' loss from 18.8 to 6.7% with an increase in the FA content from 0 to 30%, respectively.

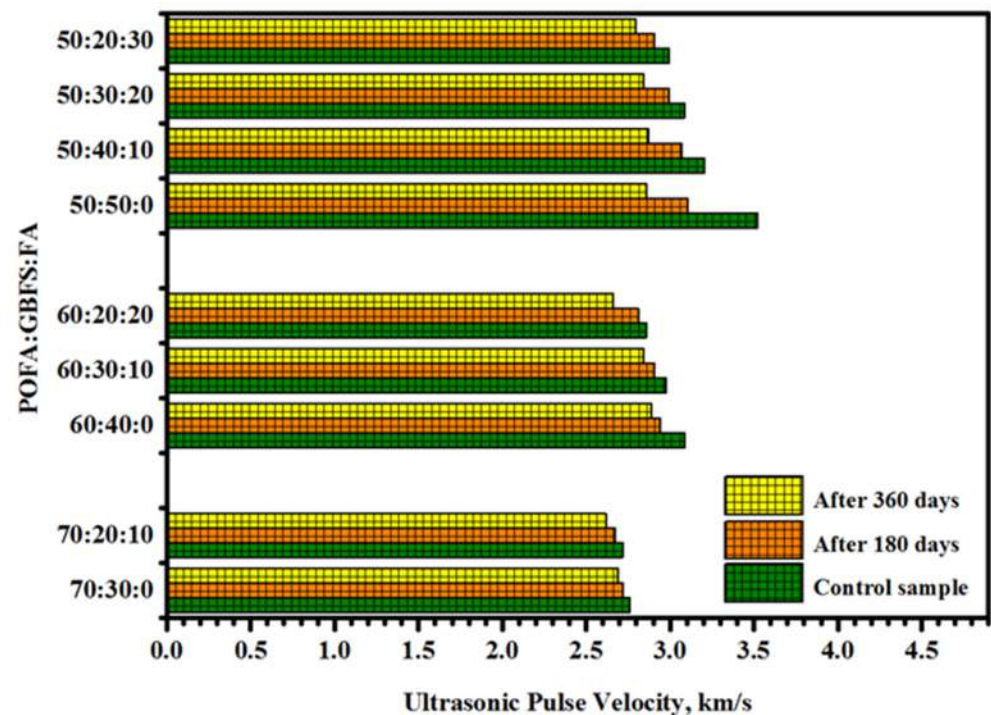


Figure 13. UPV loss of AAMs containing high level of POFA after 10%  $H_2SO_4$  solution exposure.

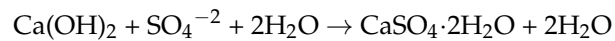
Figure 14 clearly revealed the positive effect of a high POFA content on enhancing the durability performance of the proposed mortars in terms of resistance to sulphuric acid. From the virtual appearance, the increasing POFA content from 0% (Figure 14a) to 50 to 70% (Figure 14d) and how the edges' deterioration and the number and width of the cracks reduced with an increasing amount of POFA as GBFS replacement can be seen. The increased POFA and FA content in geopolymer matrixes has affected the reduction in the calcium hydroxide content and restricted the gypsum product [48,71,72].

As per the general consensus [73–75], gypsum ( $CaSO_4 \cdot 2H_2O$ ) is produced by the reaction between a  $SO_4^{2-}$  ion and the  $Ca(OH)_2$  compound mixed in mortar following the latter's exposure to sulphuric acid. An expansive compound ettringite ( $3CaO \cdot Al_2O_3 \cdot 3CaSO_4 \cdot 32H_2O$ ) is subsequently generated following the  $Ca_4AlH_{13}$  within the mortar samples reacting with the gypsum. The softening or expansion of the alkali-activated mortar samples is possible, as the production of gypsum and expansive ettringite, which are explicated in equations one and two, can cause sulphate attacks, as per many academics. The UPV findings (Figure 13) mirrored the formation of cracks inside the sample that were triggered by expansion in the alkali-activated matrix [43]. An increased level of gypsum was found when the samples containing 50% POFA were also exposed to high levels of calcium, in contrast with the other matrixes. Thus, it is no surprise that the sample with low levels of



POFA lost over two thirds of its CS while being significantly less resistant to sulphuric acid attacks. Moreover, decreased degradation and weight loss were observed when the alkali-activated matrix contained higher levels of POFA, demonstrating how the aforementioned pattern also applies to weight loss. It was reported [73,76,77] that the low calcium alkali-activated materials have been repeatedly observed to exhibit high acid resistance, making them promising materials for applications in the aforementioned environments. There are exceptions to this general trend, i.e., unsatisfactory or ambiguous results for acid resistance tests have been reported too [78–80]. The following reactions path can explain the acid attack mechanisms:

Path I:



Path II:

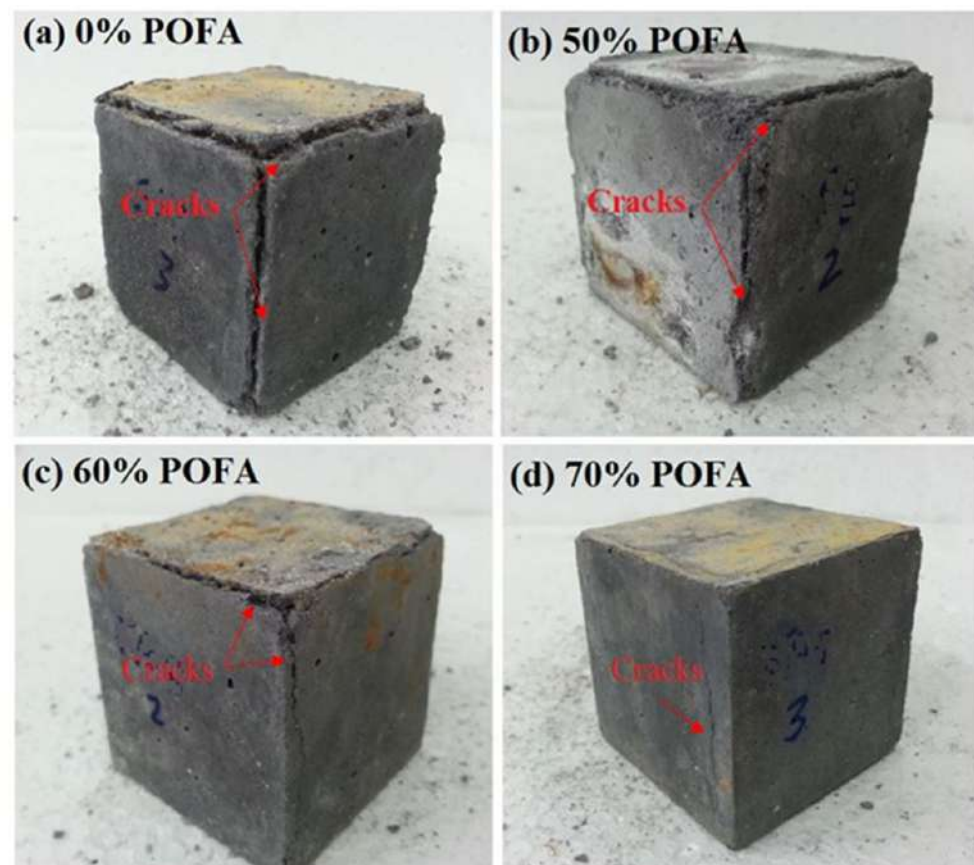
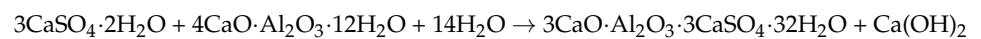


**Figure 14.** Virtual appearance of AAMs containing high level of POFA after 10%  $\text{H}_2\text{SO}_4$  solution exposure for 360 days (a) 0% POFA (b) 50% POFA (c) 60% POFA (d) 70% POFA.

The resistance of alkali-activated material specimens exposed to  $\text{H}_2\text{SO}_4$  solutions with a concentration of 3% were examined to ascertain the level of degradation [76]. The coagulation of melting fly ash particles produces sizeable ash particles that make up bottom ash. Following a period of 120 days, under 3.6% of the mass was lost in the alkali-activated high silica specimens, demonstrating a better performance than other samples. Conversely, 95.7% of the mass was lost in the high calcium content specimens after 120 days where they were almost entirely annihilated. The high calcium binder hydration structure was found to be more volatile than the cross-linked aluminosilicate structure of the high silica binder-based concrete specimens, which explains the difference in performance between the two. The impact of  $\text{H}_2\text{SO}_4$  on high calcium concrete and blended ash concrete was

compared in an academic work with regard to their resistance [71]. Sodium silicate and sodium hydroxide were utilized to activate the mix of palm oil fuel ash and fly ash that made up the blended ash concrete. In comparison with the high calcium concrete, CS loss and mass loss were counteracted more effectively by the blended ash concrete. Following a period of a year and a half, the PC concrete displayed a mass loss of 20%, while the blended ash concrete demonstrated a mass loss of 8%. Analogously, the high calcium concrete demonstrated a CS loss of 68%, while the blended ash concrete displayed a CS loss of 35%.

Cement pastes made up of equivalent quantities of GBFS and FA that were impacted by HNO<sub>3</sub> acid attacks were examined in an academic work [81]. H<sub>3</sub>O<sup>+</sup> and H<sup>+</sup> ions present within the acid solution substitute sodium and calcium ions as part of the acid attack mechanism. Additionally, Si–O–Al bonds were assaulted by acid protons in an electrophilic attack. The aluminosilicate network has its aluminium removed from it as a result. A flawed and highly siliceous structure arises due to silicon atoms substituting the aluminium. Low and high concentrations of H<sub>2</sub>SO<sub>4</sub> were applied to the mentioned mixtures to examine their resistance [82]. An HNO<sub>3</sub> acid attack was found to be equivalent to the mechanism seen at high concentrations of pH 1. Nonetheless, within the corroded layer, gypsum crystals were produced following the reaction of counter-diffusing sulphate ions with diffusing calcium ions. Increased degradation was prevented by the shielding impact of the deposited gypsum crystals within the corroded layer. The mechanism of HNO<sub>3</sub> acid attacks was found to be identical to the degradation mechanism at lower concentrations of pH 3 [82]. To what extent fly ash geopolymer pastes exposed to sulphuric acid were impacted by slag content was examined in another study [83]. Resistance to acid was signified by the corroded depth. The corroded depth of the fly ash geopolymer paste was 3 mm when the slag replaced 50% of the fly ash, while the depth was 6 mm without the slag, following 28 days of immersion. The incorporation of the slag led to a decrease in pore size and permeability, thus, diminishing the corroded depth. Sulphuric acid attack resistance in diverse blends of slag and fly ash were investigated in a separate academic work [75]. Following a period of 56 days, insignificant alterations to the mass were observed in fly ash geopolymers with a 0, 10 and 30% slag content. Nonetheless, AAS specimens exposed to sulphuric acid experienced an increase in mass that was equivalent to the mass increase when the binder contained 50% slag [79]. A mass loss of over 30% was experienced by the parallel PC specimens. Following a period of 28 days or 56 days of exposure, every specimen demonstrated substantial losses in CS. Slag and fly ash blends subjected to sulphuric acid attacks degrade due to two principal reasons [75]. One of the reasons is that the water absorption rate and permeable voids are linked to sulphate-penetration-induced corrosion. The ratio of slag to fly ash utilized determines the scale of the second cause of corrosion, which affects the reaction products.

Figure 15 presents the impact of a high volume of POFA (50, 60 and 70%) as a GBFS substitution in AAMs after being exposed to a 10% H<sub>2</sub>SO<sub>4</sub> solution for 360 days. The AAM prepared with 50% POFA revealed the dominant crystal phases plus gypsum, quartz and reinhardbraunsite. The observed intense diffraction peaks at 26.8°, 40° and 50° were due to the crystalline phase of SiO<sub>2</sub> in the mortar. The emergence of new XRD peaks at 12.8°, 16°, 20.7° and 22.4° for the AAM enclosing 50% POFA corresponded to gypsum and gismondine crystals. Other new peaks at 30.9° and 31.4° were due to the crystal phases of reinhardbraunsite. Mortars containing POFA of 60 and 70% did not show any considerable changes in the XRD patterns after the immersion in sulphuric acid solution. In short, the XRD results clearly showed a significant improvement in the mortars resistance against a sulphuric acid attack due to the inclusion of a high content of POFA as a GBFS substitute. A correlation between the resistance against a sulphuric acid attack and POFA contents as a substitute for GBFS was established.

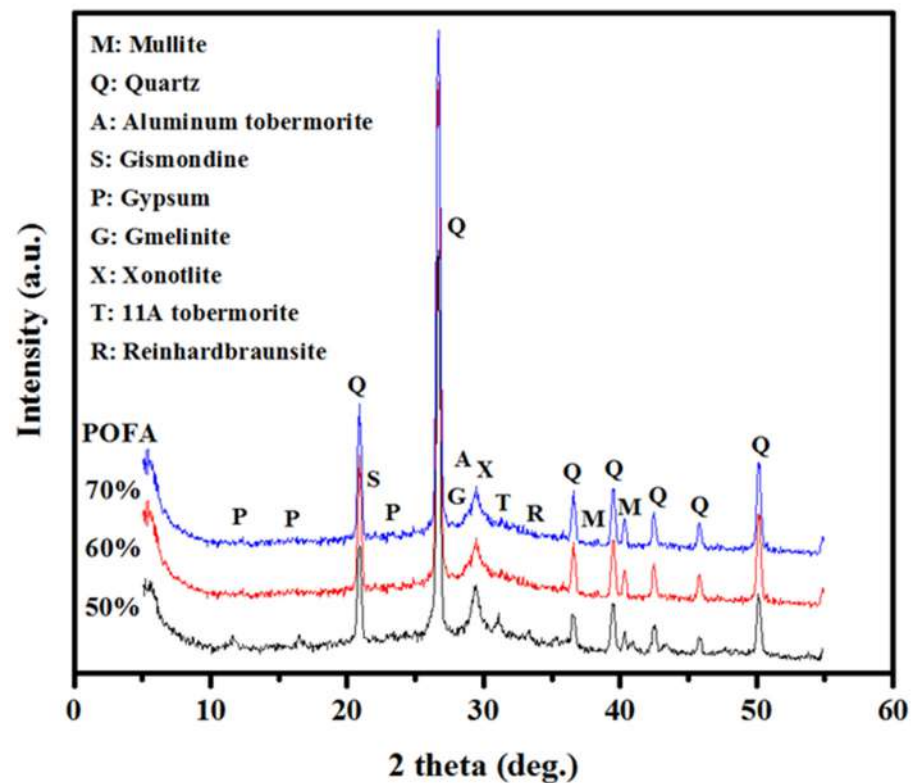


**Figure 15.** XRD patterns of 50, 60 and 70% POFA as GBFS replacement after 360 days exposed to 10% sulphuric acid.

### 3.4. Resistance to Sulphate Attack

Figure 16 shows the resistance of AAMs with a high volume of POFA content against a sulphate attack in terms of strength loss percentage. The results indicated a reduction in strength loss with an increased POFA content from 50 to 70%. For all the AAMs, the deterioration trend was increased with the increase in exposure time to 180 and 360 days. At 180 days, the rise of the POFA content from 50 to 70% as a GBFS replacement led to a reduction in the strength loss percentage from 34.8 to 14.9%, respectively. The specimens evaluated after 360 days showed the same trend of results, and the loss on strength dropped from 35.2 to 21.4% with an increasing replacement of GBFS by POFA from 50 to 70%, respectively. In each level of POFA, replacing the GBFS with FA positively enhanced the resistance of the prepared specimens to a sulphate attack and reduced the loss of strength. For the 50% POFA specimen, the loss of strength after 360 days dropped from 35.2 to 28.1% with the increase in the level of FA used as a GBFS replacement from 0 to 30%. For the 60% and 70% POFA, a similar trend was observed, and with the increasing level of FA used as a GBFS replacement, a reduction in strength loss was observed. Mortar containing 70% POFA, 20% GBFS and 10% FA displayed the highest resistance among other designed AAMs mixtures and showed strength loss of 7.7 and 15.5% after 180 and 360 days of exposure to sulphate solution, respectively. The reduction in the GBFS content with the increasing POFA and FA content led to a reduction in the loss of strength.

The effects of a high volume of POFA content and FA as a GBFS replacement on the weight loss of AAMs specimens' exposure to a sulphate solution for 180 and 360 days are illustrated in Figure 17. At 360 days, the results show that increasing the POFA content used as a GBFS replacement from 50 to 60 and 70% led to a reduction in the deterioration and weight loss percentage from 0.58 to 0.41 and 0.33, respectively. In each level of POFA, it was found that replacing GBFS with FA led to a reduction in the loss of weight and an enhancement of the durability performance. For the 50% POFA specimens' exposure to 10%  $MgSO_4$  for 360 days, the reduction in GBFS content by replacing it with FA from 50 to 20% affected the drop in weight loss percentage from 0.58 to 0.28, respectively.

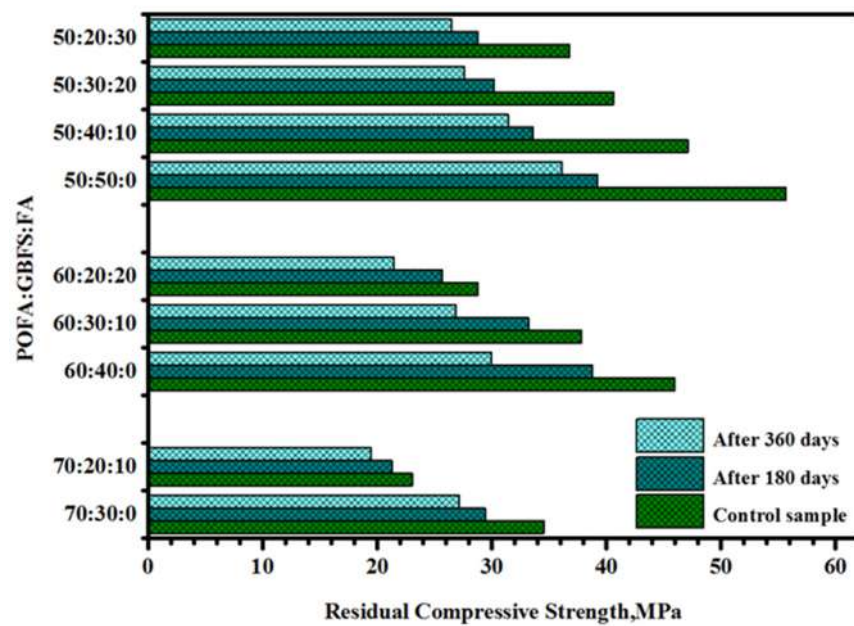


Figure 16. Residual CS of AAMs containing a high level of POFA after 10%  $MgSO_4$  solution exposure.

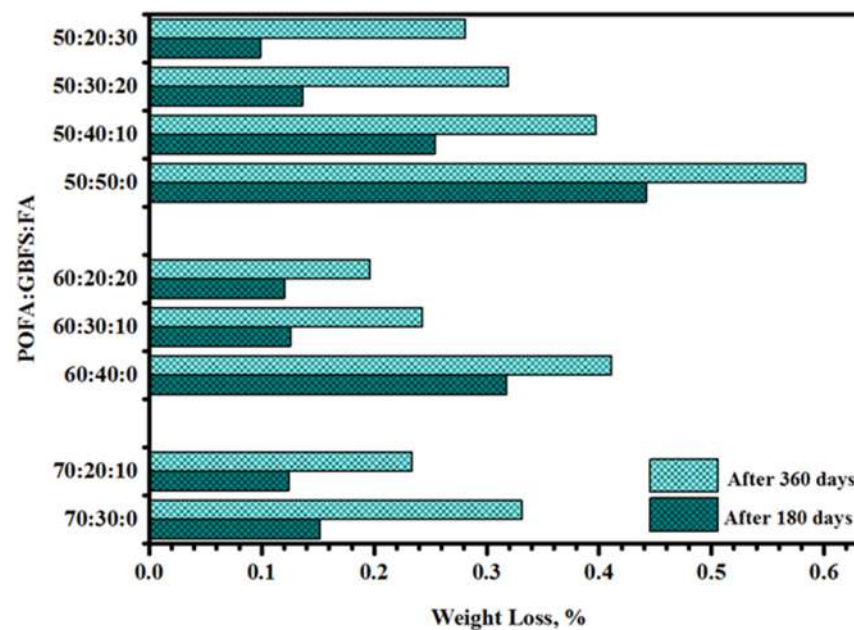


Figure 17. Weight loss of AAMs containing high level of POFA after 10%  $MgSO_4$  solution exposure.

The effects of a high volume of POFA and FA replacing GBFS on UPV readings loss percentage for AAMs are depicted in Figure 18. The increase in the content of POFA and the reduction in GBFS in the mortar led to the development of less UPV loss, internal cracks and surface scaling. The included POFA content in an alkali-activated matrix with 50, 60 and 70% led to the enhancement of the resistance of specimens and a reduction in the internal cracks; the specimens prepared with 60 and 70% POFA as a GBFS replacement and evaluated after 360 days displayed lower UPV loss (4.1 and 2.6%) compared to the 50% POFA specimens (4.3%). Similar to the strength and weight loss results, replacing GBFS with FA led to a reduction in the internal cracks and loss in UPV readings. The AAM designed with 50% POFA and exposed to a sulphate solution for 360 days showed a decrease in the UPV loss from 4.3 to 3.3% with the corresponding increase in GBFS substitution by FA from 0 to 30%. The AAMs' surface displayed high resistance to a sulphate attack and less deterioration compared to that one exposed to a sulphuric acid

attack (Figure 13). However, the results show that when increasing the POFA content from 0 (Figure 19a) to 70% (Figure 19d), the surface cracks reduce, and no deterioration appears on the surface.

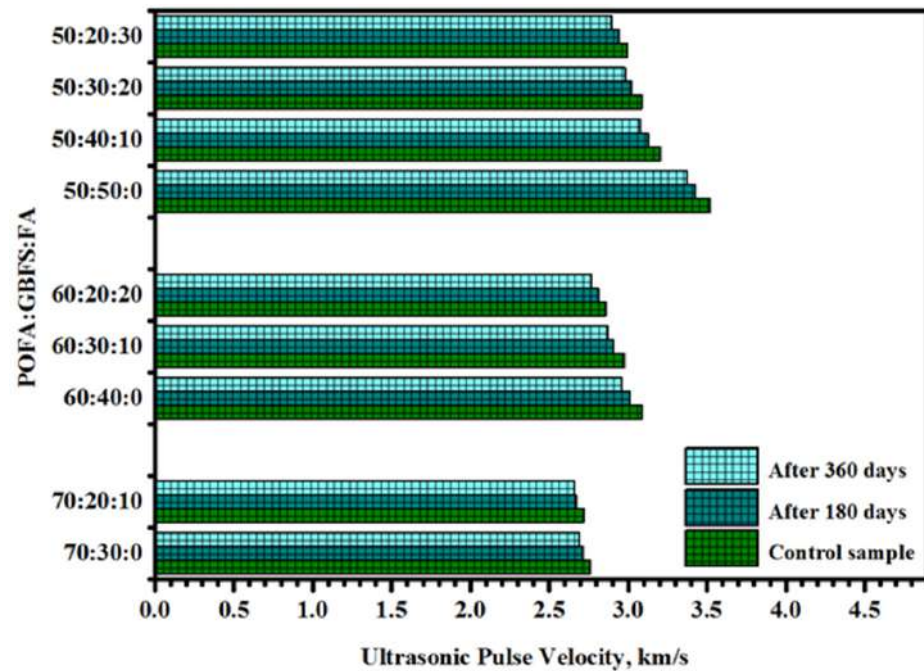


Figure 18. UVP of AAMs with high level of POFA after 10%  $MgSO_4$  solution exposure.

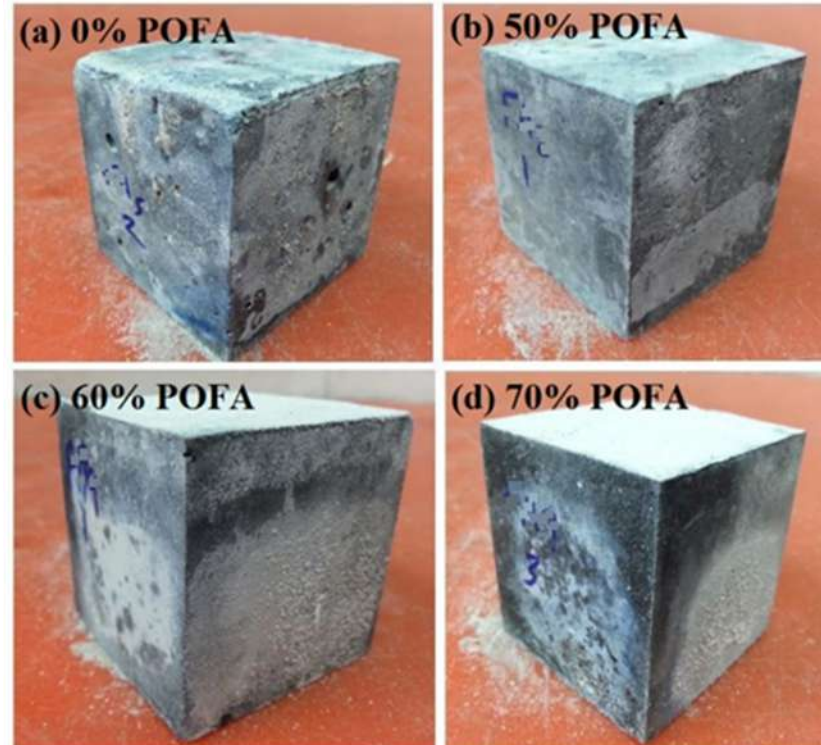


Figure 19. Effect of POFA content on the surface texture of AAMs after 10%  $MgSO_4$  solution exposure. (a) 0% POFA (b) 50% POFA (c) 60% POFA (d) 70% POFA.

Several researchers [84–86] have reported that deterioration can cause strength loss, expansion, the spalling of surface layers and, finally, disintegration. Most experts attribute a sulphate attack to the formation of expansive ettringite ( $3CaO \cdot Al_2O_3 \cdot 3CaSO_4 \cdot 32H_2O$ ) and

gypsum (calcium sulphate dehydrate ( $\text{CaSO}_4 \cdot 2\text{H}_2\text{O}$ )), which may be accompanied by the expansion or softening of AAMs. One study by Bakharev [87] found the good performance of a high silica materials (FA)-based geopolymer in sodium and magnesium sulphate solutions and attributed this to a more stable cross-linked alumina-silicate polymer structure. The high porous structure of hardened AAMs was due to an acid attack on  $\text{Ca}(\text{OH})_2$ , calcium sulfo-aluminates and the C-S-H gel containing a high amount of  $\text{CaO}/\text{SiO}_2$  in the high calcium paste. Conversely, the acid attack on the gel with a low amount of  $\text{CaO}/\text{SiO}_2$  produced some protective layers [88,89]. The OPC-based mortars prepared with pozzolans such as FA and rice husk ash were reported to be more durable against a sulphate attack than the conventional OPC mortars due to the high Ca content [90].

Figure 20 illustrates the XRD profiles of AAMs designed with a high volume of POFA as a GBFS replacement after the exposure to a 10%  $\text{MgSO}_4$  solution for 360 days. The AAMs specimens containing 50% POFA as a GBFS replacement displayed the dominant crystal phases plus gypsum and quartz. The intense diffraction peaks at  $26.8^\circ$ ,  $40^\circ$  and  $50^\circ$  were due to the crystal phases of  $\text{SiO}_2$  in AAMs. The occurrence of new XRD peaks at  $12.8^\circ$ ,  $16^\circ$ ,  $20.7^\circ$  and  $22.4^\circ$  for the mortar designed with 50% POFA were due to the crystal phase of gypsum and gismondine. The additional peaks at  $30.9^\circ$  and  $31.4^\circ$  were due to the crystal phases of reinhardbraunsite. AAMs prepared with 60 and 70% POFA did not exhibit any considerable changes in the XRD patterns after their immersion in a sulphate solution. Briefly, the XRD results of the AAMs containing a high amount of POFA as a GBFS substitution showed significant enhancement in the resistance against a sulphate attack. A correlation was determined between the rate of deterioration under the exposure of a sulphate solution and POFA contents as a substitute to GBFS.

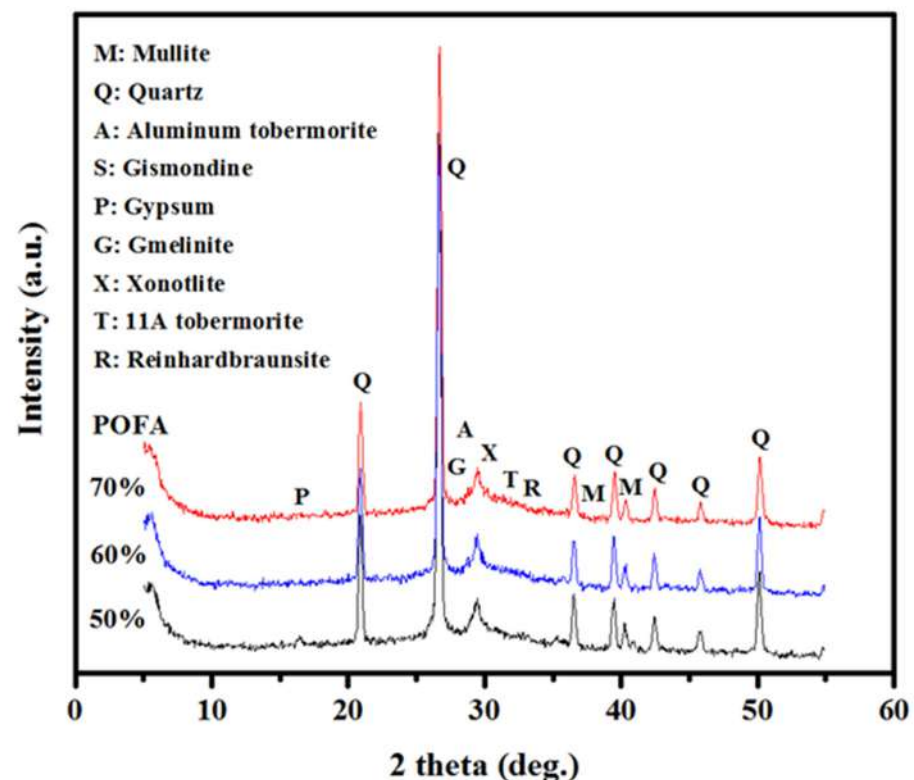


Figure 20. XRD profiles of AAMs showing the effect of various POFA levels as GBFS substitutions after being exposing to a 10% acid solution for 360 days.

#### 4. Conclusions

The effects of high volumes of POFA, GBFS and FA on the durability performance of AAMs, such as DS, and resistance to sulphuric acid and sulphate attack were eval-

uated. The detail analyses of the obtained experimental data allowed us to draw the following conclusions:

The CS of AAMs was dropped with the increase in the level of POFA used as a GBFS replacement from 50 to 70%. At every POFA level, the replacement of GBFS with FA showed a loss of strength. The low CaO content of POFA and FA negatively affected formulation C–(A)–S–H gels, which led to the achievement of lower CS.

The XRD, SEM and FTIR spectral data analyses of AAMs showed a decrease in the dense gel formation and changes in the crystallinity with the increase in the POFA contents in the mortar's matrix.

The inclusion of a high volume of POFA in the AAMs improved the durability performance in terms of the internal stress, micro-cracks and DS reduction.

The AAMs exposed to a 10% sulphuric solution showed an enhancement in the resistance to  $\text{SO}_4^{-2}$  attack with an increasing amount of POFA and FA in the alkali-activated matrix. Specimens containing high volumes of POFA (70%) and FA (10%) presented a lower loss of strength, weight and UVP readings compared to the other samples.

The virtual appearance tests showed that the deterioration in the edges and texture surface of AAMs tend to decrease with an increasing POFA content in the mortar matrix.

The results of the XRD patterns revealed that the formulation of gypsum and ettringite were restricted with the increase in the POFA content as a GBFS replacement in the matrix when exposed to a 10% sulphuric acid solution.

The residual strength, loss of weight, UVP, virtual appearance and XRD data showed an improvement in the AAMs resistance against a sulphate attack with the increase in the POFA content in the alkali-activated matrix.

The proposed AAMs were established to be excellent materials for diverse construction applications due to their environmental friendliness, sustainability and high durability.

Through the systematic preparation of new alkali-activated blends and their thorough characterizations, it was demonstrated that such ternary blends can offer the flexibility to achieve good mechanical properties and durability in order to meet the required specifications of construction industries. It was established that the exploitation of this new alkali-activated blend could promote both the economic and environmental sustainability of the construction industry.

**Author Contributions:** G.F.H.: Conceptualization, Methodology, Writing—Original draft preparation; M.A.A.: Conceptualization, Supervision; A.A.A.: Manuscript structure verification and overall research supervision, Project administration, Supervision; S.K.G.: Visualization, Supervision, Writing—review and editing; H.K.H.: Visualization, Validation; O.B.: Visualization, Validation; J.M.: Visualization, Validation, Supervision. All authors have read and agreed to the published version of the manuscript.

**Funding:** The authors extend their appreciation to Researchers Supporting Project number (RSP-2021/343), King Saud University, Riyadh, Saudi Arabia.

**Institutional Review Board Statement:** Not applicable.

**Informed Consent Statement:** Not applicable.

**Data Availability Statement:** Data is contained within the article.

**Acknowledgments:** The authors would like to thank Universiti Teknologi Malaysia (UTM), the Ministry of Higher Education, and laboratory staff for their support while completing this paper.

**Conflicts of Interest:** The authors declare no conflict of interest.

## Abbreviations

POFA	Palm oil fuel ash
GBFS	Ground blast furnace slag
FA	Fly ash
AAMs	Alkali-activated mortars
BSA	Biogenic sulphuric acid
C-S-H	Calcium silicate hydrate
CO <sub>2</sub>	Carbon dioxide
OPC	Ordinary Portland cement
MK	Metakaolin
WCP	Waste ceramic
AABs	Alkali-activated binders
CS	Compressive strength
DS	Drying shrinkage
LOI	Loss on ignition
XRF	X-ray fluorescence
XRD	X-ray diffraction
NH	Sodium hydroxide
NS	Sodium silicate
FTIR	Fourier transform infrared

## References

- Hossain, M.M.; Karim, M.R.; Hossain, M.K.; Islam, M.N.; Zain, M.F.M. Durability of mortar and concrete containing alkali-activated binder with pozzolans: A review. *Constr. Build. Mater.* **2015**, *93*, 95–109. [[CrossRef](#)]
- Huseien, G.F.; Sam, A.R.M.; Shah, K.W.; Mirza, J.; Tahir, M.M. Evaluation of alkali-activated mortars containing high volume waste ceramic powder and fly ash replacing GBFS. *Constr. Build. Mater.* **2019**, *210*, 78–92. [[CrossRef](#)]
- Mohammadhosseini, H.; Yatim, J.M.; Sam, A.R.M.; Awal, A.A. Durability performance of green concrete composites containing waste carpet fibers and palm oil fuel ash. *J. Clean. Prod.* **2017**, *144*, 448–458. [[CrossRef](#)]
- Samadi, M.; Huseien, G.F.; Mohammadhosseini, H.; Lee, H.S.; Lim, N.H.A.S.; Tahir, M.M.; Alyousef, R. Waste ceramic as low cost and eco-friendly materials in the production of sustainable mortars. *J. Clean. Prod.* **2020**, *266*, 121825. [[CrossRef](#)]
- Huseien, G.F.; Shah, K.W. Durability and life cycle evaluation of self-compacting concrete containing fly ash as GBFS replacement with alkali activation. *Constr. Build. Mater.* **2020**, *235*, 117458. [[CrossRef](#)]
- Asaad, M.A.; Ismail, M.; Tahir, M.M.; Huseien, G.F.; Raja, P.B.; Asmara, Y.P. Enhanced corrosion resistance of reinforced concrete: Role of emerging eco-friendly *Elaeis guineensis*/silver nanoparticles inhibitor. *Constr. Build. Mater.* **2018**, *188*, 555–568. [[CrossRef](#)]
- Asaad, M.A.; Ismail, M.; Raja, P.B.; Khalid, N.H.A. *Rhizophora apiculata* as eco-friendly inhibitor against mild steel corrosion in 1 M HCl. *Surf. Rev. Lett.* **2017**, *24* (Suppl. 1), 1850013. [[CrossRef](#)]
- Fang, C.; Lundgren, K.; Chen, L.; Zhu, C. Corrosion influence on bond in reinforced concrete. *Cem. Concr. Res.* **2004**, *34*, 2159–2167. [[CrossRef](#)]
- Xie, Y.; Lin, X.; Pan, W.; Ji, T.; Liang, Y.; Zhang, H. Study on corrosion mechanism of alkali-activated concrete with biogenic sulfuric acid. *Constr. Build. Mater.* **2018**, *188*, 9–16. [[CrossRef](#)]
- Li, X.; Lin, X.; Lin, K.; Ji, T. Study on the degradation mechanism of sulphoaluminate cement sea sand concrete eroded by biological sulfuric acid. *Constr. Build. Mater.* **2017**, *157*, 331–336. [[CrossRef](#)]
- Asaad, M.A.; Sarbini, N.N.; Sulaiman, A.; Ismail, M.; Huseien, G.F.; Majid, Z.A.; Raja, P.B. Improved corrosion resistance of mild steel against acid activation: Impact of novel *Elaeis guineensis* and silver nanoparticles. *J. Ind. Eng. Chem.* **2018**, *63*, 139–148. [[CrossRef](#)]
- Thiebaut, Y.; Multon, S.; Sellier, A.; Lacarrière, L.; Boutillon, L.; Belili, D.; Linger, L.; Cussigh, F.; Hadji, S. Effects of stress on concrete expansion due to delayed ettringite formation. *Constr. Build. Mater.* **2018**, *183*, 626–641. [[CrossRef](#)]
- Taylor, H.; Famy, C.; Scrivener, K. Delayed ettringite formation. *Cem. Concr. Res.* **2001**, *31*, 683–693. [[CrossRef](#)]
- Odler, I.; Colán-Subauste, J. Investigations on cement expansion associated with ettringite formation. *Cem. Concr. Res.* **1999**, *29*, 731–735. [[CrossRef](#)]
- Sun, D.; Wu, K.; Shi, H.; Miramini, S.; Zhang, L. Deformation behaviour of concrete materials under the sulfate attack. *Constr. Build. Mater.* **2019**, *210*, 232–241. [[CrossRef](#)]
- Chiniforush, A.A.; Gharehchaei, M.; Nezhad, A.A.; Castel, A.; Moghaddam, F.; Keyte, L.; Hocking, D.; Foster, S. Minimising risk of early-age thermal cracking and delayed ettringite formation in concrete—A hybrid numerical simulation and genetic algorithm mix optimisation approach. *Constr. Build. Mater.* **2021**, *299*, 124280. [[CrossRef](#)]
- Gao, Z.; Zhang, P.; Guo, J.; Wang, K. Bonding behavior of concrete matrix and alkali-activated mortar incorporating nano-SiO<sub>2</sub> and polyvinyl alcohol fiber: Theoretical analysis and prediction model. *Ceram. Int.* **2021**, *47*, 31638–31649. [[CrossRef](#)]



18. Huseien, G.F.; Sam, A.R.M.; Alyousef, R. Texture, morphology and strength performance of self-compacting alkali-activated concrete: Role of fly ash as GBFS replacement. *Constr. Build. Mater.* **2021**, *270*, 121368. [[CrossRef](#)]
19. Mohammadhosseini, H.; Lim, N.H.A.S.; Tahir, M.M.; Alyousef, R.; Alabduljabbar, H.; Samadi, M. Enhanced performance of green mortar comprising high volume of ceramic waste in aggressive environments. *Constr. Build. Mater.* **2019**, *212*, 607–617. [[CrossRef](#)]
20. Al-Fasih, M.Y.M.; Huseien, G.F.; bin Ibrahim, I.S.; Sam, A.R.M.; Algaifi, H.A.; Alyousef, R. Life-Cycle Assessment of Alkali-Activated Materials Incorporating Industrial Byproducts. *Materials* **2021**, *14*, 2401.
21. Mhaya, A.M.; Baghban, M.H.; Faridmehr, I.; Huseien, G.F.; Abidin, A.R.Z.; Ismail, M. Performance Evaluation of Modified Rubberized Concrete Exposed to Aggressive Environments. *Materials* **2021**, *14*, 1900. [[CrossRef](#)] [[PubMed](#)]
22. Faridmehr, I.; Bedon, C.; Huseien, G.F.; Nikoo, M.; Baghban, M.H. Assessment of mechanical properties and structural morphology of alkali-activated mortars with industrial waste materials. *Sustainability* **2021**, *13*, 2062. [[CrossRef](#)]
23. Van den Heede, P. *Durability and Sustainability of Concrete with High Volumes of Fly Ash*; Ghent University: Ghent, Belgium, 2014.
24. Coppola, L.; Coffetti, D.; Crotti, E. Pre-Packed alkali activated cement-free mortars for repair of existing masonry buildings and concrete structures. *Constr. Build. Mater.* **2018**, *173*, 111–117. [[CrossRef](#)]
25. Gómez-Casero, M.A.; Pérez-Villarejo, L.; Castro, E.; Eliche-Quesada, D. Effect of steel slag and curing temperature on the improvement in technological properties of biomass bottom ash based alkali-activated materials. *Constr. Build. Mater.* **2021**, *302*, 124205. [[CrossRef](#)]
26. Zhang, B.; Zhu, H.; Shah, K.W.; Feng, P.; Dong, Z. Optimization of mix proportion of alkali-activated slag mortars prepared with seawater and coral sand. *Constr. Build. Mater.* **2021**, *284*, 122805. [[CrossRef](#)]
27. Zhang, B.; Zhu, H.; Shah, K.W.; Dong, Z.; Wu, J. Performance evaluation and microstructure characterization of seawater and coral/sea sand alkali-activated mortars. *Constr. Build. Mater.* **2020**, *259*, 120403. [[CrossRef](#)]
28. Huseien, G.; Ismail, M.; Tahir, M.; Mirza, J.; Hussein, A.; Khalid, N.; Sarbini, N. Effect of binder to fine aggregate content on performance of sustainable alkali activated mortars incorporating solid waste materials. *Chem. Eng. Trans.* **2018**, *63*, 667–672.
29. Rafeet, A.; Vinai, R.; Soutsos, M.; Sha, W. Effects of slag substitution on physical and mechanical properties of fly ash-based alkali activated binders (AABs). *Cem. Concr. Res.* **2019**, *122*, 118–135. [[CrossRef](#)]
30. Mondal, S.K.; Welz, A.; Rownaghi, A.; Wang, B.; Ma, H.; Rezaei, F.; Kumar, A.; Okoronkwo, M.U. Investigating the microstructure of high-calcium fly ash-based alkali-activated material for aqueous Zn sorption. *Environ. Res.* **2021**, *198*, 110484. [[CrossRef](#)]
31. Goma, E.; Sargon, S.; Kashosi, C.; Gheni, A.; ElGawady, M.A. Mechanical properties of high early strength class c fly Ash-Based alkali activated concrete. *Transp. Res. Rec.* **2020**, *2674*, 430–443. [[CrossRef](#)]
32. Adam, A.A. *Strength and Durability Properties of Alkali Activated Slag and Fly Ash-Based Geopolymer Concrete*; RMIT University: Melbourne, Australia, 2009.
33. De Vargas, A.S.; Dal Molin, D.C.; Vilela, A.C.; Da Silva, F.J.; Pavao, B.; Veit, H. The effects of Na<sub>2</sub>O/SiO<sub>2</sub> molar ratio, curing temperature and age on compressive strength, morphology and microstructure of alkali-activated fly ash-based geopolymers. *Cem. Concr. Compos.* **2011**, *33*, 653–660. [[CrossRef](#)]
34. Farhan, N.A.; Sheikh, M.N.; Hadi, M.N. Investigation of engineering properties of normal and high strength fly ash based geopolymer and alkali-activated slag concrete compared to ordinary Portland cement concrete. *Constr. Build. Mater.* **2019**, *196*, 26–42. [[CrossRef](#)]
35. Huseien, G.F.; Mirza, J.; Ismail, M.; Ghoshal, S.K.; Hussein, A.A. Geopolymer mortars as sustainable repair material: A comprehensive review. *Renew. Sustain. Energy Rev.* **2017**, *80*, 54–74. [[CrossRef](#)]
36. Lim, N.H.A.S.; Mohammadhosseini, H.; Tahir, M.M.; Samadi, M.; Sam, A.R.M. Microstructure and strength properties of mortar containing waste ceramic nanoparticles. *Arab. J. Sci. Eng.* **2018**, *43*, 5305–5313. [[CrossRef](#)]
37. Mhaya, A.M.; Huseien, G.F.; Faridmehr, I.; Abidin, A.R.Z.; Alyousef, R.; Ismail, M. Evaluating mechanical properties and impact resistance of modified concrete containing ground Blast Furnace slag and discarded rubber tire crumbs. *Constr. Build. Mater.* **2021**, *295*, 123603. [[CrossRef](#)]
38. Faridmehr, I.; Huseien, G.F.; Baghban, M.H. Evaluation of mechanical and environmental properties of engineered alkali-activated green mortar. *Materials* **2020**, *13*, 4098. [[CrossRef](#)]
39. Chen, Z.; You, N.; Chen, C.; Zhang, Y. Properties of dredged sludge solidified with alkali-activated slag-based materials and blended with copper slag as fine aggregates of mortars. *Constr. Build. Mater.* **2021**, *312*, 125459. [[CrossRef](#)]
40. Samadi, M.; Huseien, G.F.; Lim, N.H.A.S.; Mohammadhosseini, H.; Alyousef, R.; Mirza, J.; Abd Rahman, A.B. Enhanced performance of nano-palm oil ash-based green mortar against sulphate environment. *J. Build. Eng.* **2020**, *32*, 101640. [[CrossRef](#)]
41. Chen, C.; Habert, G.; Bouzidi, Y.; Jullien, A. Environmental impact of cement production: Detail of the different processes and cement plant variability evaluation. *J. Clean. Prod.* **2010**, *18*, 478–485. [[CrossRef](#)]
42. Zhang, P.; Wang, K.; Li, Q.; Wang, J.; Ling, Y. Fabrication and engineering properties of concretes based on geopolymers/alkali-activated binders—A review. *J. Clean. Prod.* **2020**, *258*, 120896. [[CrossRef](#)]
43. Huseien, G.F.; Tahir, M.M.; Mirza, J.; Ismail, M.; Shah, K.W.; Asaad, M.A. Effects of POFA replaced with FA on durability properties of GBFS included alkali activated mortars. *Constr. Build. Mater.* **2018**, *175*, 174–186. [[CrossRef](#)]
44. Lim, N.H.A.S.; Ismail, M.A.; Lee, H.S.; Hussin, M.W.; Sam, A.R.M.; Samadi, M. The effects of high volume nano palm oil fuel ash on microstructure properties and hydration temperature of mortar. *Constr. Build. Mater.* **2015**, *93*, 29–34. [[CrossRef](#)]
45. Mohammadhosseini, H.; Awal, A.A.; Ehsan, A.H. Influence of palm oil fuel ash on fresh and mechanical properties of self-compacting concrete. *Sadhana* **2015**, *40*, 1989–1999. [[CrossRef](#)]

46. Khankhaje, E.; Hussin, M.W.; Mirza, J.; Rafieizonooz, M.; Salim, M.R.; Siong, H.C.; Warid, M.N.M. On blended cement and geopolymer concretes containing palm oil fuel ash. *Mater. Des.* **2016**, *89*, 385–398. [[CrossRef](#)]
47. Muthusamy, K.; Mirza, J.; Zamri, N.A.; Hussin, M.W.; Majeed, A.P.A.; Kusbiantoro, A.; Budiea, A.M.A. Properties of high strength palm oil clinker lightweight concrete containing palm oil fuel ash in tropical climate. *Constr. Build. Mater.* **2019**, *199*, 163–177. [[CrossRef](#)]
48. Huseien, G.F.; Ismail, M.; Tahir, M.M.; Mirza, J.; Khalid, N.H.A.; Asaad, M.A.; Husein, A.A.; Sarbini, N.N. Synergism between palm oil fuel ash and slag: Production of environmental-friendly alkali activated mortars with enhanced properties. *Constr. Build. Mater.* **2018**, *170*, 235–244. [[CrossRef](#)]
49. Mohammadhosseini, H.; Ngian, S.P.; Alyousef, R.; Tahir, M.M. Synergistic effects of waste plastic food tray as low-cost fibrous materials and palm oil fuel ash on transport properties and drying shrinkage of concrete. *J. Build. Eng.* **2021**, *42*, 102826. [[CrossRef](#)]
50. Hamada, H.M.; Thomas, B.S.; Yahaya, F.M.; Muthusamy, K.; Yang, J.; Abdalla, J.A.; Hawileh, R.A. Sustainable use of palm oil fuel ash as a supplementary cementitious material: A comprehensive review. *J. Build. Eng.* **2021**, *40*, 102286. [[CrossRef](#)]
51. Alnahhal, A.M.; Alengaram, U.J.; Yusoff, S.; Singh, R.; Radwan, M.K.; Deboucha, W. Synthesis of sustainable lightweight foamed concrete using palm oil fuel ash as a cement replacement material. *J. Build. Eng.* **2021**, *35*, 102047. [[CrossRef](#)]
52. Awal, A.A.; MHussin, W. The effectiveness of palm oil fuel ash in preventing expansion due to alkali-silica reaction. *Cem. Concr. Compos.* **1997**, *19*, 367–372. [[CrossRef](#)]
53. Awal, A.A.; Mohammadhosseini, H. Green concrete production incorporating waste carpet fiber and palm oil fuel ash. *J. Clean. Prod.* **2016**, *137*, 157–166. [[CrossRef](#)]
54. Tangchirapat, W.; Saeting, T.; Jaturapitakkul, C.; Kiattikomol, K.; Siripanichgorn, A. Use of waste ash from palm oil industry in concrete. *Waste Manag.* **2007**, *27*, 81–88. [[CrossRef](#)] [[PubMed](#)]
55. Güneyisi, E.; Gesoğlu, M.; Mermerdaş, K. Improving strength, drying shrinkage, and pore structure of concrete using metakaolin. *Mater. Struct.* **2008**, *41*, 937–949. [[CrossRef](#)]
56. Alsubari, B.; Shafiqh, P.; Jumaat, M.Z. Development of self-consolidating high strength concrete incorporating treated palm oil fuel ash. *Materials* **2015**, *8*, 2154–2173. [[CrossRef](#)]
57. Tay, J.-H. Ash from oil-palm waste as a concrete material. *J. Mater. Civ. Eng.* **1990**, *2*, 94–105. [[CrossRef](#)]
58. Awal, A.A.A.A.A.; Hussin, M.H.M. Strength, modulus of elasticity and shrinkage behaviour of POFA concrete. *Malays. J. Civ. Eng.* **2009**, *21*, 125–134.
59. Hossain, M.M.; Karim, M.R.; Elahi, M.M.A.; Islam, M.N.; Zain, M.F.M. Long-term durability properties of alkali-activated binders containing slag, fly ash, palm oil fuel ash and rice husk ash. *Constr. Build. Mater.* **2020**, *251*, 119094. [[CrossRef](#)]
60. Tangchirapat, W.; Jaturapitakkul, C. Strength, drying shrinkage, and water permeability of concrete incorporating ground palm oil fuel ash. *Cem. Concr. Compos.* **2010**, *32*, 767–774. [[CrossRef](#)]
61. Lim, N.H.A.S.; Samadi, M.; Sam, A.R.M.; Abd Khalid, N.H.; Sarbini, N.N.; Ariffin, N.F.; Hussin, M.W.; Ismail, M.A. Drying Shrinkage of Mortar Incorporating High Volume Oil Palm Biomass Waste. In Proceedings of the E3S Web of Conferences, Kuala Lumpur, Malaysia, 2–5 October 2018; EDP Sciences: Les Ulis, France, 2018; Volume 34, p. 01008.
62. Farzadnia, N.; Noorvand, H.; Yasin, A.M.; Aziz, F.N.A. The effect of nano silica on short term drying shrinkage of POFA cement mortars. *Constr. Build. Mater.* **2015**, *95*, 636–646. [[CrossRef](#)]
63. Testing, A.S.F.; Cement, M.C.C.-O. *Standard Test Method for Compressive Strength of Hydraulic Cement Mortars (Using 2-in. Or [50-mm] Cube Specimens)*; ASTM International: West Conshohocken, PA, USA, 2013.
64. *ASTM C267-01. Standard Test Methods for Chemical Resistance of Mortars, Grouts, and Monolithic Surfacing and Polymer Concretes*; ASTM International: West Conshohocken, PA, USA, 2012; pp. 1–6.
65. Ranjbar, N.; Mehrali, M.; Alengaram, U.J.; Metselaar, H.S.C.; Jumaat, M.Z. Compressive strength and microstructural analysis of fly ash/palm oil fuel ash based geopolymer mortar under elevated temperatures. *Constr. Build. Mater.* **2014**, *65*, 114–121. [[CrossRef](#)]
66. Kubba, Z.; Huseien, G.F.; Sam, A.R.M.; Shah, K.W.; Asaad, M.A.; Ismail, M.; Tahir, M.M.; Mirza, J. Impact of curing temperatures and alkaline activators on compressive strength and porosity of ternary blended geopolymer mortars. *Case Stud. Constr. Mater.* **2018**, *9*, e00205. [[CrossRef](#)]
67. Al-Majidi, M.H.; Lampropoulos, A.; Cundy, A.; Meikle, S. Development of geopolymer mortar under ambient temperature for in situ applications. *Constr. Build. Mater.* **2016**, *120*, 198–211. [[CrossRef](#)]
68. Somna, K.; Jaturapitakkul, C.; Kajitvichyanukul, P.; Chindaprasirt, P. NaOH-Activated ground fly ash geopolymer cured at ambient temperature. *Fuel* **2011**, *90*, 2118–2124. [[CrossRef](#)]
69. Saha, A.K. Effect of class F fly ash on the durability properties of concrete. *Sustain. Environ. Res.* **2018**, *28*, 25–31. [[CrossRef](#)]
70. Makhloufi, Z.; Bederina, M.; Bouhicha, M.; Kadri, E.H. Effect of mineral admixtures on resistance to sulfuric acid solution of mortars with quaternary binders. *Phys. Procedia* **2014**, *55*, 329–335. [[CrossRef](#)]
71. Ariffin, M.A.M.; Bhutta, M.A.R.; Hussin, M.W.; Tahir, M.M.; Aziah, N. Sulfuric acid resistance of blended ash geopolymer concrete. *Constr. Build. Mater.* **2013**, *43*, 80–86. [[CrossRef](#)]
72. Huseien, G.F.; Ismail, M.; Khalid, N.H.A.; Hussin, M.W.; Mirza, J. Compressive strength and microstructure of assorted wastes incorporated geopolymer mortars: Effect of solution molarity. *Alex. Eng. J.* **2018**, *57*, 3375–3386. [[CrossRef](#)]
73. Sturm, P.; Gluth, G.J.G.; Jäger, C.; Brouwers, H.J.H.; Kühne, H.C. Sulfuric acid resistance of one-part alkali-activated mortars. *Cem. Concr. Res.* **2018**, *109*, 54–63. [[CrossRef](#)]

74. Gu, L.; Bennett, T.; Visintin, P. Sulphuric acid exposure of conventional concrete and alkali-activated concrete: Assessment of test methodologies. *Constr. Build. Mater.* **2019**, *197*, 681–692. [[CrossRef](#)]
75. Lee, N.; Lee, H.-K. Influence of the slag content on the chloride and sulfuric acid resistances of alkali-activated fly ash/slag paste. *Cem. Concr. Compos.* **2016**, *72*, 168–179. [[CrossRef](#)]
76. Sata, V.; Sathonsaowaphak, A.; Chindaprasirt, P. Resistance of lignite bottom ash geopolymer mortar to sulfate and sulfuric acid attack. *Cem. Concr. Compos.* **2012**, *34*, 700–708. [[CrossRef](#)]
77. Koenig, A.; Herrmann, A.; Overmann, S.; Dehn, F. Resistance of alkali-activated binders to organic acid attack: Assessment of evaluation criteria and damage mechanisms. *Constr. Build. Mater.* **2017**, *151*, 405–413. [[CrossRef](#)]
78. Temuujin, J.; Minjigmaa, A.; Lee, M.; Chen-Tan, N.; Van Riessen, A. Characterisation of class F fly ash geopolymer pastes immersed in acid and alkaline solutions. *Cem. Concr. Compos.* **2011**, *33*, 1086–1091. [[CrossRef](#)]
79. Aliques-Granero, J.; Tognonvi, T.; Tagnit-Hamou, A. Durability test methods and their application to AAMs: Case of sulfuric-acid resistance. *Mater. Struct.* **2017**, *50*, 1–14. [[CrossRef](#)]
80. Özcan, A.; Karakoç, M.B. The resistance of blast furnace slag-and ferrochrome slag-based geopolymer concrete against acid attack. *Int. J. Civ. Eng.* **2019**, *17*, 1571–1583. [[CrossRef](#)]
81. Allahverdi, A.; Skvara, F. Sulfuric acid attack on hardened paste of geopolymer cements—Part 1. Mechanism of corrosion at relatively high concentrations. *Ceram. Silik.* **2005**, *49*, 225.
82. Allahverdi, A.; Skvara, F. Sulfuric acid attack on hardened paste of geopolymer cements—Part 2. Corrosion mechanism at mild and relatively low concentrations. *Ceram. Silik.* **2006**, *50*, 1.
83. Lloyd, R.R.; Provis, J.L.; van Deventer, J.S. Acid resistance of inorganic polymer binders. 1. Corrosion rate. *Mater. Struct.* **2012**, *45*, 1–14.
84. Yusuf, M.O. Performance of slag blended alkaline activated palm oil fuel ash mortar in sulfate environments. *Constr. Build. Mater.* **2015**, *98*, 417–424. [[CrossRef](#)]
85. Bhutta, M.A.R.; Hussin, W.M.; Azreen, M.; Tahir, M.M. Sulphate resistance of geopolymer concrete prepared from blended waste fuel ash. *J. Mater. Civ. Eng.* **2014**, *26*, 04014080. [[CrossRef](#)]
86. Donatello, S.; Fernández-Jimenez, A.; Palomo, A. Very high volume fly ash cements. Early age hydration study using Na<sub>2</sub>SO<sub>4</sub> as an activator. *J. Am. Ceram. Soc.* **2013**, *96*, 900–906.
87. Bakharev, T. Durability of geopolymer materials in sodium and magnesium sulfate solutions. *Cem. Concr. Res.* **2005**, *35*, 1233–1246. [[CrossRef](#)]
88. Khatri, R.; Sirivivatnanon, V.; Yang, J. Role of permeability in sulphate attack. *Cem. Concr. Res.* **1997**, *27*, 1179–1189. [[CrossRef](#)]
89. Ngo, S.H.; Huynh, T.P.; Le, T.T.; Mai, N.H.T. Effect of high loss on ignition-fly ash on properties of concrete fully immersed in sulfate solution. In Proceedings of the IOP Conference Series: Materials Science and Engineering, Nanjing, China, 17–19 August 2018; IOP Publishing: Bristol, UK, 2018; Volume 371, p. 012007.
90. Hamzah, H.K.; Huseien, G.F.; Asaad, M.A.; Georgescu, D.P.; Ghoshal, S.K.; Alrshoudi, F. Effect of waste glass bottles-derived nanopowder as slag replacement on mortars with alkali activation: Durability characteristics. *Case Stud. Constr. Mater.* **2021**, *15*, e00775. [[CrossRef](#)]